Bernal-Sanchez, J., McDougall, J., Barreto, D., Dimitriadi, V., Leak, J., & Anbazhagan, P. (2025). Influence of rubber content and particle morphology on the dynamic behaviour, liquefaction susceptibility and internal stability of shredded rubber-sand mixtures. *Geosynthetics International*, 1-21. Advance online publication. https://doi.org/10.1680/jgein.24.00157. For the purpose of open access, a CC BY 4.0 licence has been applied.

Influence of rubber content and particle morphology on the dynamic behaviour, liquefaction susceptibility and internal stability of Shredded Rubber-Sand mixtures

J. Bernal-Sanchez[1], J. McDougall[2], D. Barreto[3], V. Dimitriadi[4], J. Leak[5], P. Anbazhagan[6]

[1]*Lecturer in Civil Engineering, School of Engineering & the Built Environment, Edinburgh Napier University, Merchiston Campus, 10 Colinton Road, EH10 5DT, United Kingdom, E-mail: J.Bernal-Sanchez@napier.ac.uk (corresponding author)*

[2]*Reader in Geotechnical Engineering, School of Engineering & the Built Environment, Edinburgh Napier University, Merchiston Campus, 10 Colinton Road, EH10 5DT, United Kingdom, E-mail: J.McDougall@napier.ac.uk*

[3]*Associate Professor in Geotechnical Engineering, School of Engineering & the Built Environment, Edinburgh Napier University, Merchiston Campus, 10 Colinton Road, EH10 5DT, United Kingdom, E-mail: D.Barreto@napier.ac.uk*

[4]*Lecturer in Geotechnical Engineering, School of Engineering & the Built Environment, Edinburgh Napier University, Merchiston Campus, 10 Colinton Road, EH10 5DT, United Kingdom, E-mail: V.Dimitriadi@napier.ac.uk*

[5]*Teaching Associate in Geotechnical Engineering, Department of Civil & Geoenvironmental Engineering, Strathclyde University, James Weir Building, Montrose St, Glasgow G1 1XQ, United Kingdom, E-mail: james.leak@strath.ac.uk*

[6]*Professor in Geotechnical Engineering, Department of Civil Engineering, Indian Institute of Science, Bangalore 560012, India, E-mail: anbazhagan@iisc.ac.in*

ABSTRACT: Understanding the resilience of Rubber-Soil mixtures (RSm) under cyclic loading is crucial for their application in seismic isolation. This study presents an investigation into the dynamic behaviour, internal stability, and liquefaction resistance of Shredded Rubber Sand mixtures (ShRSm) under both short and long-term cyclic loading conditions. Key material properties including rubber content, size ratio, and particle shape were compared with existing literature. Utilising resonant column and cyclic triaxial apparatus, an experimental programme was conducted across small to large strain amplitudes, applying up to 400 strain-controlled cycles. The findings reveal that mixtures with larger or elongated rubber particles exhibit greater stiffness degradation but also higher damping capacity. Incorporating at least 10% Shredded Rubber (ShR) significantly enhances internal stability, reduces stiffness degradation under strains up to 1%, and mitigates pore water pressure buildup,

Bernal-Sanchez, J., McDougall, J., Barreto, D., Dimitriadi, V., Leak, J., & Anbazhagan, P. (2025). Influence of rubber content and particle morphology on the dynamic behaviour, liquefaction susceptibility and internal stability of shredded rubber-sand mixtures. *Geosynthetics International*, 1-21. Advance online publication. https://doi.org/10.1680/jgein.24.00157. For the purpose of open access, a CC BY 4.0 licence has been applied.

thereby improving liquefaction resistance. While sand-like soils display higher initial energy dissipation that decays under loading, rubber-like soils maintain consistent damping over long-term cyclic conditions. These results not only advance the understanding of RSm in seismic applications but also demonstrate that ShRSm is a viable and sustainable material for permanent Geotechnical Seismic Isolation (GSI) technology, with the potential to influence engineering practices in earthquake-prone regions.

Keywords: Geosynthetics**,** Rubber-Soil mixtures, Shredded Rubber Sand mixtures (ShRSm), Consolidated undrained cyclic triaxial tests, Small-to-Large deformations, Stiffness and damping degradation, Dynamic behaviour, Geotechnical Seismic Isolation systems (GSI), Earthquakes.

1 INTRODUCTION

Earthquakes rank among the deadliest natural disasters. Since 1990, an average of 17 major earthquakes with a magnitude above 7 have occurred annually, resulting in approximately 27,000 deaths each year (Spence and Scawthorn, 2011). Most fatalities occur in densely populated urban areas in developing countries, primarily due to substandard construction materials and inadequate urban planning (Guha-Sapir et al., 2016). Although base isolation methods have mitigated earthquake damage (Kelly and Van Engelen, 2015), their implementation is challenging and costly, especially for low-to-medium-rise buildings in developing regions.

Geotechnical Seismic Isolation (GSI) systems offer an alternative to traditional structural isolation methods by altering soil conditions through flexible or sliding interfaces in contact with geological sediments (Tsang, 2008; 2009; 2012). The concept of using Rubber-Soil mixtures (RSm) for seismic isolation was first introduced by Tsang (2008), while the term GSI was formally defined in Tsang (2009). Notably, Tsang (2008) demonstrated that GSI-RSm can mitigate not only horizontal seismic shaking but also vertical ground motion effects, further enhancing its potential for earthquake protection applications. Thereafter, RSm have been adopted in the literature as a potential geomaterial to reduce the impact of seismic motions due to their potential capacity to offset destructive disturbances, primarily strong horizontal accelerations (Hazarika et al., 2008; Tsang and Pitilakis, 2019; Tsang et al., 2020). Despite their benefits, the recycling of vulcanised rubber is complex, leading to the disposal of used tires in landfills or stockpiles. Only 3.7% of recovered tyres in Europe are used in civil engineering projects (ETRMA, 2015). New applications, such as the one proposed in this study, are needed to offer alternative uses for recovered tires and reduce health risks associated with their use as derived fuel.

The behaviour of RSm under various loading regimes is challenging to understand due to the incorporation of deformable rubber particles. This study explores how rigid and flexible particles interact, influencing macroscopic behaviour based on material properties like rubber content, size ratio (SR = d_{R50}/d_{S50}) and shape (Kim and Santamarina, 2008; Fonseca et al., 2019; Bernal-Sanchez et al., 2023). While RSm shows increased compressibility compared to traditional mineral soils (Masad et al., 1996; Youwai and Bergado, 2003), when it comes to strength, the situation is less straightforward. In static conditions, the shear resistance may either rise, with the inclusion of larger tyre chips or shreds (Zornberg et al., 2004; Rao and Dutta, 2006; Mashiri et al., 2015), or may fall, with the inclusion of rubber crumbs or small fibres (Edincliler et al., 2010; Sheikh et al., 2012; Fu et

al., 2017). The shear strength behaviour is thus known to be governed by various material properties including rubber mass, size, shape, and stiffness, and how they interact with sand particles (Bernal-Sanchez et al., 2020). Lee et al. (2007, 2010) postulated the concepts of sand-like behaviour, i.e. mixtures exhibiting a higher small-to-large strain shear stiffness, and rubber-like behaviour, i.e. mixtures with lower shear moduli that deform more easily under loading, to explain the evolution in the macro-scale parameters of RSm. This study refers to these terms to explain the evolution in the dynamic properties of the studied materials.

Understanding both static and dynamic behaviour of soils is crucial in geotechnical earthquake and offshore engineering. The dynamic behaviour of geomaterials, such as RSm, primarily depends on shear modulus (G) and damping ratio (ξ). Unlike static behaviour, dynamic testing involves factors like frequency and number of cycles, which influence G and ξ. These properties must be characterised at various strain levels under both dry and saturated conditions to reflect on-site behaviour (Towhata, 2014; Bernal-Sanchez, 2020). The dynamic behaviour of RSm has typically been characterised into two main groups. One focuses on small-to-medium deformations using bender element tests (Lee et al., 2010) or resonant column tests (Feng and Sutter, 2000; Anastasiadis et al., 2012a-b; Senetakis et al., 2012). The other group concentrates on medium-to-large strains via cyclic triaxial tests (Nakhaei et al., 2012; Eshani et al., 2015; Li et al., 2016; Pistolas et al., 2018). All the previous studies agree that the proportion of rubber, the sand-rubber SR, and the rubber shape (e.g. aspect ratio, thickness), seem to directly influence the evolution of both G and ξ.

The literature generally agrees that the small-strain shear stiffness of RSm increases with confining pressure but decreases with rubber content and shear strain amplitude (Anastasiadis et al., 2012b). This reduction in stiffness is less pronounced in sand-like behaviour, observed at lower rubber contents (below 35%) and with larger rubber particles (Lee et al., 2007; Lee et al., 2010). Additionally, a more linear stiffness degradation (G/G_0) occurs under cyclic loading at small-to-large strains with higher rubber contents (Anastasiadis et al., 2012a; Senetakis et al., 2012; Pistolas et al., 2018). This pattern aligns with the transition from sand-like to rubber-like behaviour observed in the literature (Lee et al., 2007; Kim and Santamarina, 2008). Regarding damping capacity, minimum damping ratio increases with rubber content at any stress level due to friction between sand particles and rubber deformation (Feng and Sutter, 2000). However, predicting damping at medium-to-large strains is challenging. At high stresses ($\sigma > 200$kPa), damping is largely unaffected by SR (Ehsani et al. 2015, Li et al., 2016). At lower stresses, damping capacity varies with rubber size, shape, and content (Nakhaei et al., 2012; Pistolas et al., 2018).

Bernal-Sanchez et al. (2018) introduced the first dynamic characterisation of shredded rubber-sand mixtures (ShRSm) using resonant column and cyclic triaxial tests, focusing on short-term behaviour across various rubber contents. Bernal-Sanchez (2020) extended this work offering a detailed examination of the long-term cyclic response of RSm, including liquefaction resistance, strain-dependent stiffness degradation, and recovery mechanisms under varying amplitudes and cycle counts. Bernal-Sanchez et al. (2022, 2024) applied these findings in a GSI context, demonstrating the potential of RSm layers to attenuate seismic energy transfer in foundation systems, and proposing implementation strategies for GSI design. Bernal-Sanchez et al. (2023) introduced a grading entropy-based framework to evaluate the effect of particle size distribution on the stiffness and

liquefaction susceptibility of RSm, offering a probabilistic interpretation of mechanical behaviour. Alternatively, Liu et al. (2023) showed that RSm cored composite blocks reduce seismic displacement and enhance energy dissipation, making them a cost-effective solution for rural housing applications. Wu et al. (2023) highlighted that RSm cushions provide enhanced seismic isolation performance depending on site conditions, with factors such as thickness and base pressure playing a crucial role in optimising their effectiveness. Furthermore, Wang et al. (2024) validated that soilbags filled with RSm effectively dampen high-frequency seismic waves, offering a scalable and adaptable seismic isolation solution, particularly for low-rise structures.

Recent research has emphasised the importance of grading characteristics in governing the mechanical and dynamic behaviour of RSm. Fiamingo et al. (2025a) conducted monotonic triaxial tests on well-graded gravel–rubber mixtures and showed that the inclusion of shredded rubber, at volumetric contents up to 55%, maintained appreciable shear strength while significantly enhancing energy absorption capacity, suggesting greater suitability of well graded mixtures for practical GSI applications compared to poorly graded counterparts. Their follow-up work also highlighted the influence of confining pressure and volumetric thresholds on the transition from rigid gravel-like to soft rubber-like responses (Fiamingo et al., 2025b). At the dynamic scale, Banzibaganye and Vrettos (2022) performed resonant column tests on sands of varying gradations mixed with coarse tyre chips, deriving prediction equations for normalised shear modulus and damping as a function of chip content and confining stress. Their results demonstrated that uniform medium sands were more sensitive to rubber addition than poorly graded sands, evidencing the role of soil skeleton arrangement. Kowalska and Vrettos (2024) compared layered versus mixed sand–rubber configurations in resonant column tests and found that layered specimens behave closer to pure rubber, with very low shear modulus and higher damping than uniform mixtures of the same rubber fraction. This line of work underscores that gradation, well-graded versus uniform, and configuration, layered versus mixed, may alter both strength and small-strain stiffness, thereby informing mixture design and field implementation strategies for GSI systems.

Although most seismic events are of lower magnitudes, magnitude seven earthquakes can induce soils to exhibit medium-to-large strains ($\gamma > 0.2\%$) for durations exceeding ten seconds (Nazari et al., 2014; Towhata, 2014). Under strong motions, strains exceeding 1% are commonly recorded (Kokusho, 1980; Kumar et al., 2017). Therefore, understanding the dynamic properties of geomaterials under large strains is crucial for their application in critical infrastructure, e.g. offshore foundations, soil embankments, excavations, slopes, earth dams, and dikes. Specifically, the study of G and ξ are vital for GSI systems, which depend on the ability of materials like RSm to deform and dissipate energy (Tsang et al., 2020; Vratsikidis and Pitilakis, 2022; Bernal-Sanchez et al., 2022). While evidence suggests that stiffness and damping are influenced by the number of cycles at strains as low as 0.15% (El Shamy and Denissen, 2012; Kumar et al., 2013; 2017), few studies have examined the evolution of these properties in RSm across a broad strain range (< 0.5%) (Mashiri et al., 2016; Madhusudhan et al., 2019). Additionally, most studies have focused on irregular scrap tires with varying rubber-sand SR (Kaneko et al., 2013; Mashiri et al., 2016; Pistolas et al., 2018), leaving a gap in understanding the dynamic response of mixtures with similar sized rubber and sand particles over extended deformations.

Bernal-Sanchez, J., McDougall, J., Barreto, D., Dimitriadi, V., Leak, J., & Anbazhagan, P. (2025). Influence of rubber content and particle morphology on the dynamic behaviour, liquefaction susceptibility and internal stability of shredded rubber-sand mixtures. *Geosynthetics International*, 1-21. Advance online publication. https://doi.org/10.1680/jgein.24.00157. For the purpose of open access, a CC BY 4.0 licence has been applied.

Additionally, previous research has shown that incorporating tire-derived aggregates can reduce Pore Water Pressure (PWP) and enhance liquefaction resistance under saturated conditions (Hazarika et al., 2006; Kaneko et al., 2013; Mashiri et al., 2016). However, outcomes vary depending on material properties. For instance, tire shreds improve damping capacity and PWP mitigation, while tire powder is more effective in managing pressure build-up (Bahadori and Manafi, 2015; Bahadori and Farzalizadeh, 2018). Conversely, high-density mixtures with tire chips or granulated rubber have shown decreased liquefaction resistance (Promputthangkoon and Hyde, 2007; Shariatmadari et al., 2018). Bernal-Sanchez et al. (2023) highlighted the importance of Particle Size Distribution (PSD) for the internal stability of rubber-containing mixtures but noted limitations in the stability criterion due to unaccounted particle characteristics and test conditions.

This study addresses the aforementioned gaps by investigating the impact of short-term, understood as a small number of cycles, versus long-term conditions, i.e. numerous cycles accounting for seismic aftermath, on the dynamic behaviour, internal stability, and liquefaction susceptibility of RSm. It aims to elucidate how variations in material properties, strain amplitude and cycle number influence PWP build-up and liquefaction resistance of RSm, providing a more comprehensive understanding of RSm suitability for permanent GSI systems.

2 EXPERIMENTAL INVESTIGATION

2.1 Materials

This study employs a mix of Leighton Buzzard sand (LBS) and rubber from recycled car tires. All the information corresponding to material properties of LBS and particulate rubber can be found in Table 1. The sand is coarse and rounded to sub-rounded (Fig. 1b), with an average particle size of d_{S50}=0.85 mm, a coefficient of uniformity C_u=1.27, specific gravity G_s=2.68, and PSD as depicted in Figure 1a. According to ASTM D6270-12, tyre-derived aggregate (TDA) includes tyre shreds and tyre chips, which are rectangular pieces of scrap tyres ranging between 12 mm and 305 mm in size. Tyre shreds typically fall within the 50–305 mm range, while tyre chips, which have most of the wire removed, range between 12–50 mm. These larger aggregates are often used in civil engineering applications such as lightweight fill, drainage layers, and energy absorption structures due to their high porosity and compressibility. On the other hand, particulate rubber refers to finer rubber particles obtained through mechanical size reduction processes. This category includes granulated rubber (425 μm – 12 mm), ground rubber (425 μm – 2 mm), and buffing rubber, which is generated from the removal of tread during the tyre retreading process. These smaller particles are often used in geotechnical applications, rubberized asphalt, and composite materials due to their improved workability and distribution within mixtures.

The rubber fines used in this study are distinct from both TDA and other particulate rubbers due to their small particle size and high surface area which result from producing tyre shreds. Their finer gradation ensures a more homogeneous distribution within soil matrices. The recycled rubber of this study, sourced from car tire sidewalls after removal of steel belts, underwent devulcanization and mechanical shredding to achieve the desired particle size range, with an average particle size of d_{R50}=1.62 mm (as shown in Figure 1a). In this study, rubber fines of a similar size to LBS were selected to optimise gradation compatibility and reduce particle segregation, which can

occur when materials of significantly different sizes are mixed. This ensured a more uniform distribution within the soil matrix, enhancing compaction efficiency and improving the mechanical performance of the mixture.

These rubber fines resembling small shreds (Figure 1c) are henceforth referred to as Shredded Rubber (ShR), characterised by a low specific gravity G_s=1.12 (Edil and Bosscher, 1994; Sheikh et al., 2012). The specific gravity of both soil and rubber particles was determined using the pycnometer method in accordance with ASTM D854. Friction coefficients were assigned based on values from the literature: $\mu = 0.24$ for Leighton Buzzard Sand (LBS) and $\mu = 1.0$ for shredded rubber, as reported by Senetakis et al. (2013) and Lopera Perez et al. (2016).

To ensure representative sampling and adequate specimen volume, ShR particles were obtained from ten independent batches supplied by the same manufacturer. This common origin resulted in relatively consistent particle size and morphology across batches. Particle shape was characterised using three descriptors: sphericity, reflecting similarity to a sphere; roundness, indicating the smoothness of edges and corners; and aspect ratio, defined as the ratio of the longest to shortest dimension, capturing elongation or flatness. Shape characterisation followed the image-based procedure of Cho et al. (2006), with measurements taken using ImageJ software. Given the uniformity of the particle size distribution, ten measurements per batch were sufficient, and variations in sphericity and roundness were within ±5% of their mean values. Aspect ratio ranged between 2 and 6.

Manual inspection during preparation confirmed that particles were elongated and angular, with visible surface fissures. These features were documented through stereoscopic microscopy (Fig. 1d), and microfissures were further confirmed by Scanning Electron Microscopy. Microscopic imaging also revealed high surface porosity and the presence of cracks, which are believed to facilitate localised strain accumulation and energy dissipation during cyclic loading. Although fissure density was not quantified statistically, their consistent presence across batches supports their role in the mechanical response of ShR. As shown in Table 1, the mixtures of LBS and shredded rubber fibres (ShRSm) exhibited a relatively similar size ratio, with SR, i.e. $d_{R50}/d_{S50} = 1.88$.

The rubber content in this study is primarily defined based on mass. This approach ensures compatibility with existing research on the behaviour of RSm, where rubber content is predominantly reported in terms of weight percentage (Anastasiadis et al., 2012b; Ehsani et al., 2015). Adopting this standardised methodology facilitates direct comparisons with previous studies, enhancing the reproducibility and contextual relevance of the results. The mixtures studied in this manuscript were prepared adding 0%, 10%, 20%, and 30% rubber by weight.

The minimum and maximum densities of LBS and ShRSm were calculated according to BS 1377-4 (1990). For minimum density (ρ_{min}), LBS samples were allowed to fall freely in a glass cylinder to maximise voids. For ShRSm, 2.5% moisture was added to avoid segregation. Ten tests were performed on each specimen, and the average values are shown in Figure 2a. Maximum density (ρ_{max}) was determined by compacting the samples with a vibrating hammer. Each sample was divided into three equal layers. A circular tamper was positioned on top of the mould, and each layer was compacted using a vibrating hammer for 2 minutes. The vibrating hammer used had a mass of 10 kg and operated at a frequency of approximately 200 Hz, delivering a consistent downward force of 400 N. These parameters conform to BS 1377-4 (1990) and ASTM D7382-08 specifications. The highest dry

Bernal-Sanchez, J., McDougall, J., Barreto, D., Dimitriadi, V., Leak, J., & Anbazhagan, P. (2025). Influence of rubber content and particle morphology on the dynamic behaviour, liquefaction susceptibility and internal stability of shredded rubber-sand mixtures. *Geosynthetics International*, 1-21. Advance online publication. https://doi.org/10.1680/jgein.24.00157. For the purpose of open access, a CC BY 4.0 licence has been applied.

mass from two tests per material was used to determine ρ_{max} (Figure 2a). LBS specimens were tested underwater, while ShRSm specimens were tested in moist conditions to prevent floating due to the low specific gravity (G_s = 1.12). It was determined that a moisture content of 2.5% was optimal for compacting ShRSm. This specific moisture level was selected based on preliminary trials, which indicated a higher degree of compaction while preventing the segregation of finer sand particles to the bottom of the mould.

A consistent reduction in dry density (Fig. 2a) is observed with increasing rubber percentage, which aligns with expectations given the significantly lower density of rubber compared to sand. Interestingly, the difference between maximum and minimum dry densities is relatively small for pure sand (χ = 0%) and pure rubber (χ = 100%), but this difference becomes more pronounced for intermediate rubber percentages. This trend can be attributed to the interaction between sand and rubber particles, which alters the packing efficiency of the mixture. At low rubber contents, rubber particles tend to occupy voids within the sand matrix, leading to a moderate decrease in dry density. However, as rubber content increases, the rubber particles progressively disrupt the natural packing of sand grains, introducing additional voids and increasing the heterogeneity of the mixture. The greater disparity between loose and dense states at intermediate rubber contents (e.g., χ = 10 – 50%) suggests that rubber's compressibility and irregular shape play a role in reducing packing efficiency. As rubber content approaches 100%, the mixture behaves more like pure rubber, exhibiting a more stable dry density range.

Figure 2b shows the dry densities and maximum (e_{max}) and minimum (e_{min}) void ratios for each mixture. Increasing rubber content increases e_{max}, while e_{min} remains nearly constant. The equivalent void ratio (e_{eq}), proposed by previous studies (Feng and Sutter, 2000; Anastasiadis et al., 2012a), reflects the reduction in soil stiffness due to low rubber stiffness. Unlike traditional void ratio calculations, e_{eq} includes the volume occupied by rubber (V_r) in the total void volume (V_v), while only the sand volume contributes to stiffness (V_s), calculated as follows:

$$e_{eq} = \frac{V_v + V_r}{V_s} \quad (1)$$

As shown in Figure 2b, e_{eq} increases more rapidly than e_{max}, consistent with the literature (Pistolas et al., 2018), and it is recommended to analytically calculate dynamic soil stiffness of RSm (Bernal-Sanchez et al., 2020).

2.2 Equipment

The dynamic properties of ShRSm at very small-to-medium strains were investigated using a resonant column/torsional (RC) shear testing apparatus (GCTS TSH-200), which can vibrate the soil specimen at frequencies up to 250 Hz with a torque capacity of 2.3 Nm and pneumatic pressure fluid. The Computer Aided Testing System (i.e., CATS) available offered a digitalised servo control over the sensors and transducers of the system. Experimental data recording was completed via GCTS control software installed in the equipment. Recorded data were: time, torque (Nm), back pressure (kPa), confining pressure (kPa), pore water pressure (kPa), acceleration (g), and phase shift (rad). One thousand data points per second per variable were stored.

For medium-to-large strains, a cyclic triaxial (CT) testing rig was used, operating within a frequency range of 0.01 Hz to 10 Hz. This rig includes a 50 kN capacity loading frame with a pneumatic actuator capable of double

amplitude axial displacements up to 25 mm. Precise displacement monitoring was ensured by adopting an integrated linear variable differential transformer transducer, accurate to 0.001 mm. Additionally, the equipment includes three standard pressure transducers to measure variations in cell pressure, PWP, and back pressure. Data acquisition was carried out as frequently as the resonant test by means of the software DYNATRIAX. Recorded data were time (s), confining pressure (kPa), back pressure (kPa), axial load (kN), pore water pressure (kPa), change in pore water pressure (u) and vertical displacement (mm). A detailed chapter on the equipment used and procedures followed can be found in Bernal-Sanchez (2020).

2.3 Methods

Specimens for both RC and CT testing were prepared with a diameter of 50 mm and height of 100 mm, giving a 2:1 aspect ratio in accordance with ASTM D3999 and ASTM D4015. This geometry is designed to reduce end restraint and ensure uniform stress distribution. The maximum shredded rubber particle length (≈6 mm) was smaller than one-fifth of the specimen diameter, consistent with recommendations for dynamic testing. Boundary influences were further minimised by the use of porous stones, lubricated platens, and controlled with consistent sample preparation later explained. While no segregation or gradation change was observed during or after testing, the elongated morphology and fissures of ShR may introduce local anisotropy that is not fully captured in small laboratory specimens. This highlights the need for complementary large-scale or field testing to validate small-strain laboratory results for engineering application.

The procedure for introducing ShRSm into the rubber membrane was adapted from the dry deposition method proposed in the literature (ASTM D698; Ishihara, 1996). Wet deposition method was discarded due to the small rubber particles floating and affecting the homogeneity and consistency of sample preparation. Due to the elongated shape of ShR used in this study, which prevented placement through a funnel-shaped cone, a modified approach was necessary. To minimise segregation of the smaller sand particles during sample preparation, a moisture content of 2.5% was maintained. This practice aligns with findings by Li et al. (2016), who addressed sand segregation issues under dry conditions. The addition of a small amount of moisture creates negative pore pressures, helping to hold particles in place against gravitational forces during pouring.

Both sample height and the overall volume (200 cm^3) were maintained consistently across all samples. As the rubber content increased, the sand and rubber proportions were adjusted to preserve the rubber-to-sand mass ratio determined by gravimetric analysis. To ensure uniformity, the material was mixed, divided into equal portions, and after introduced into a latex membrane-lined mould in four distinct layers. A uniform, light tamping was applied to each layer until an initial height of 25 mm was reached for the first layer, and the process was continued until the final sample height was achieved. This compaction method ensured a consistent material distribution and minimised density variations, thereby enhancing the reliability of the experimental results.

Saturation was achieved using the back pressure saturation method (ASTM D7181-11). De-aired water was introduced through the PWP valve, circulated through the sample, and extracted via the back pressure valve while

maintaining a 20 kPa cell pressure. Saturation was completed by gradually increasing the cell and back pressure until a Skempton pore-pressure parameter B ($\Delta U/\Delta\sigma$) of 0.95 was reached.

As observed in Table 2 regarding the experimental programme, the relative density (D_r) of 65–85% was selected to reflect expected field conditions for GSI applications and other civil engineering uses of granular materials. In engineering practice, medium-to-dense states are typically achieved to ensure sufficient stiffness, shear strength, and liquefaction resistance in soils subjected to dynamic loading. According to Jensen (2024) and Krogh et al. (2022), siliceous sands in offshore and seismic geotechnical applications commonly exhibit relative densities above 60%, with improved performance in the 65–85% range, making this selection relevant for seismic resilience studies. This range is also consistent with prior studies on RSm (Nakhaei et al., 2012; Rouhanifar et al., 2020), where medium-to-dense compaction states were found to optimise energy dissipation and reduce liquefaction susceptibility. Nakhaei et al. (2012) observed that rubber-sand mixtures compacted to $D_r \geq 65\%$ exhibited lower shear modulus degradation and increased liquefaction resistance compared to looser specimens. Similarly, Rouhanifar et al. (2020) found that in cyclic triaxial tests, D_r values between 70–85% resulted in enhanced stiffness retention over multiple loading cycles, further justifying the selection in this study.

2.4 Test programme

Small-strain deformations ($\gamma < 0.01\%$), investigated using RC tests, are relevant to low-intensity dynamic loads, such as traffic vibrations, wind loading on structures, and microtremors from minor seismic activity (Kramer, 1996; Towhata, 2008). In these cases, stiffness degradation and damping remain limited, and the elastic behaviour of geomaterials dominates (Feng and Sutter, 2000). Medium-to-large strain amplitudes ($\gamma = 0.05\% – 1\%$), as tested in CT experiments, correspond to strong ground shaking during earthquakes. For GSI applications, understanding the stiffness and damping evolution at these strain levels is critical, as ShRSm are intended to mitigate seismic energy dissipation and prevent soil failure under extreme cyclic loads (Tsang et al., 2020; Vratsikidis and Pitilakis, 2022).

The experimental plan involved testing ShRSm with varying rubber contents using RC and CT equipment under undrained saturated conditions. All specimens were uniformly consolidated at a confining pressure of 100 kPa. In the RC tests, the dynamic response was assessed based on peak deformation under various torque forces, ranging from 0.0034 Nm to 54.2 Nm for sand and 0.014 Nm to 5.15 Nm for the 30ShRm, covering small-to-medium shear strains (0.0001 - 0.06%) in accordance with ASTM 4015-15. During the CT tests, specimens were subjected to 400 strain-controlled loading cycles at a frequency of 1 Hz. Each test was conducted at a fixed shear strain amplitude, γ = 0.1%, 0.2%, or 1%, to represent medium-to-large strain levels. The strain amplitude was kept constant throughout the duration of each test, allowing the effects of cyclic loading on shear stiffness, damping ratio, and PWP development to be assessed independently of strain variation.

The study aims to evaluate dynamic properties of LBS and ShRSm. Shear modulus (G) and damping ratio (ξ) were determined by analysing hysteresis loops from the cyclic loads (ASTM 3999-11). For consistency, dynamic properties of ShRSm were evaluated from the second cyclic loop, focusing on stiffness and damping evolution as

Bernal-Sanchez, J., McDougall, J., Barreto, D., Dimitriadi, V., Leak, J., & Anbazhagan, P. (2025). Influence of rubber content and particle morphology on the dynamic behaviour, liquefaction susceptibility and internal stability of shredded rubber-sand mixtures. *Geosynthetics International*, 1-21. Advance online publication. https://doi.org/10.1680/jgein.24.00157. For the purpose of open access, a CC BY 4.0 licence has been applied.

a function of the number of loading cycles. Earthquakes typically involve complex load patterns, including varying amplitudes and frequencies, characterised by a main shock followed by numerous aftershocks, which collectively may impact soil behaviour significantly (Kramer, 1996; Towhata, 2008).

A total of 400 cycles was selected to capture both the short-term (N < 20 cycles) and long-term (N > 100 cycles) cyclic response of the mixtures. The extended testing was designed to reflect scenarios involving prolonged seismic shaking, strong aftershock sequences (Nazari et al., 2014), and repeated anthropogenic vibrations such as railway and traffic-induced loads (Murillo et al., 2009; Signes et al., 2017). Previous research (Mashiri et al., 2016; Li et al., 2016) has highlighted that stiffness and damping degradation in RSm may evolve beyond 100 cycles, making higher cycle counts necessary to assess cumulative effects. The choice of 400 cycles therefore provided a practical scenario, sufficient to observe the transition between short and long-term behaviour, while avoiding excessive testing durations or specimen degradation not representative of field conditions.

Liquefaction susceptibility was assessed by recording the number of cycles required for the excess pore pressure ratio to reach a value of one, which corresponds to the onset of soil liquefaction. In this study, the excess pore pressure ratio (r_u) was defined as the measured increase in pore water pressure (Δ_u) divided by the initial mean effective confining stress (σ'_m). Pore water pressure was monitored using a calibrated pressure transducer (±0.5% accuracy) located at the base of the specimen, and the signal was sampled at a frequency of 2 Hz throughout cyclic loading. The condition of liquefaction was considered to be met when this ratio reached or exceeded unity and remained at that level for at least three consecutive cycles. To confirm this threshold, pore pressure build-up was compared against strain-based signs of liquefaction, such as the sudden accumulation of large strains and the development of nearly horizontal stress–strain loops indicating the loss of effective confining stress. The concurrence of these deformation features with the point at which the pore pressure ratio reached one supports the validity of the criterion, in line with definitions of liquefaction used in cyclic triaxial testing (Ishihara, 1993; Kramer, 1996; Kaneko et al., 2013; Boulanger & Idriss, 2014).

Additional details on cyclic behaviour, including deviatoric stress and stress path evaluations at various strain amplitudes, can be found in Bernal-Sanchez et al. (2020). In the context of this study, the term "resilience" refers to the capacity of ShRSm to maintain shear stiffness, dissipate energy, and resist liquefaction across multiple cycles of cyclic loading. Therefore, it is the material-level definition which is employed, consistent with recent uses in geotechnical engineering (e.g., Qian et al., 2020; Dushmantha et al., 2025).

3 RESULTS AND DISCUSSION

3.1 Dynamic properties of ShRSm and RSm

Figures 3a-c show the changes in G, G/G_0 and ξ of ShRSm across a range of rubber contents and strains (γ = 0.0001 – 1%). Figure 3a illustrates that G decreases with increasing shear strain and rubber content. This reduction is attributed to the deformable rubber particles (Feng and Sutter, 2000; Senetakis et al., 2012; Bernal-Sanchez et al., 2018, 2020). The observed reduction in shear modulus and concurrent increase in damping ratio with increasing strain amplitude align with the strain-dependent behaviour reported by Feng and Sutter (2000), who

demonstrated that cyclic stiffness degradation in granular materials is accentuated under reduced loading frequencies due to the time-dependent deformation mechanisms. This reinforces our findings from CT tests, where lower frequencies produced greater damping and modulus reduction compared to RC tests.

In Fig. 3b, specimens with lower rubber content (χ = 0–10%) exhibit similar stiffness degradation to pure sand, with a sharper decrease in stiffness at larger strains. In contrast, specimens with higher rubber content (χ = 20–30%) show more linear normalised shear modulus curves but a more gradual reduction in G (Fig. 3a), indicating a rubber-like behaviour (Kim and Santamarina, 2008). The latter is also seen in the evolution with the rubber content of the reference strain (γ_{ref}) which expresses the deformation level at which $G/G_0 = 0.5$, and it is an indicator of the linearity of the dynamic soil behaviour (Kramer, 1996; Nakhaei et al., 2012). This suggests that ShRSm can better withstand medium-to-large strains.

Figure 3c depicts enhancements in both viscous (small strain) and hysteretic (large strain) damping with added rubber fibres. This aligns with literature (Senetakis et al., 2012) showing that energy dissipation in RSm results from both sand particle friction and rubber deformation. Within the range of γ = 0.01 – 0.1%, ξ increases linearly with rubber content. However, beyond γ = 0.1 or 0.2%, this relationship deteriorates, particularly in LBS and 10ShRSm at high strains, due to a limiting shear strain (γ_{lim}) that marks maximum damping capacity as as reported by Pistolas et al. (2018), who established an early onset of nonlinearity in modulus degradation curves, particularly at strain levels above 0.05%. This is consistent with the results in this study, where ShRSm exhibit a sharper modulus drop at $\gamma \approx 0.1\%$, highlighting the transition from elastic to plastic behaviour, especially at $\chi \geq 20\%$. This limit appears to rise with rubber content. While ξ decays at $\chi > 10\%$, sand-like specimens show an upper limit in damping, contrasting with the increasing trend in 20-30ShRSm. This phenomenon is due to the interlocking mechanism from the rearrangement of rubber and sand particles and the high coefficient of friction of rubber, known to be more pronounced in rubber-like soils (μ = 1) (Lopera Perez et al., 2016).

Figure 4 presents the normalised shear modulus degradation curves (G/G_0) as a function of shear strain for ShRSm with rubber contents of χ = 10% (Figure 4a) and χ = 30% (Figure 4b), alongside data reported in prior experimental studies. The literature sources were selected based on the similarity of their confining pressures (i.e. 50–200 kPa), rubber material properties, and testing configurations, with the key properties summarised in Table 3 to provide comparative interpretation. These include the apparatus type, rubber-to-sand SR, particle morphology, relative density, strain amplitude range, and number of cycles tested.

In Figure 4a, the mixture tested in the current study displays the greatest stiffness degradation across the entire shear strain range, particularly beyond γ = 0.01%, when compared to the other studies. This pronounced behaviour is primarily attributed to the angular and elongated shape of the ShR used (i.e., A_r = 2 - 6), which promotes early onset of nonlinearity through localised strain concentration and reduced effective confinement within the sand skeleton. In addition to their shape, the ShR particles exhibited visible fissures and microcracks on their surfaces (see Figure 1c-d), a characteristic resulting from the mechanical shredding process. These surface imperfections may act as micro-deformation zones, allowing for internal strain absorption and dissipation during cyclic loading,

thereby contributing to both the enhanced damping (as shown in Figure 5a) and the accelerated stiffness degradation observed in this mixture (Fig. 4a), further explained and evidenced in Section 3.2 of this manuscript.

By contrast, Feng and Sutter (2000) observed a more gradual stiffness degradation using rubber fibres with SR values between 4 and 6. Their resonant column tests, conducted on dense specimens (D_r = 70 - 100%), revealed high G/G_0 retention, especially at small-to-medium strains. The fibrous geometry likely promoted interlocking and stable contact chains, reducing the rate of modulus degradation compared to the present study. Nakhaei et al. (2012) used granular rubber with SR ≈ 1 in cyclic triaxial tests. Their specimens were prepared at lower relative densities, and the more spherical shape of the rubber may have facilitated particle rearrangement without abrupt stress transfer. Yet even their results indicate less stiffness loss than observed in this study, suggesting that rubber geometry and interparticle friction play a critical role in exacerbating modulus degradation. The results of Mashiri et al. (2016), using large tyre chips with SR ≈ 15, show a more moderate modulus decline, despite their use of larger rubber particles. Their specimens, compacted under static uniaxial conditions, were relatively loose (Dr = 50%) and the rubber primarily acted as a passive filler. The more gradual modulus reduction observed in their work likely reflects the dampening effect of the larger, softer rubber phase, rather than a structural weakening of the sand skeleton. In the case of Pistolas et al. (2018), who employed granulated rubber with SR = 4-8, the degradation curve aligns more closely with this study at medium strains ($\gamma \approx 0.01$–0.1%). However, their curve still sits above the results of this study, suggesting that the use of highly angular ShR, combined with a medium-to-dense sand matrix, results in a more fragile contact network under increasing strain amplitudes.

In Figure 4b, at $\chi = 30\%$ the trend becomes more consistent with literature and the modulus degradation observed in this study aligns more closely with the curves of Kaneko et al. (2013) and Pistolas et al. (2018) at large strains. As the volumetric content of rubber increases, the role of rubber-to-rubber contacts becomes more dominant, producing a nonlinear response that is common across several studies. The data from Anastasiadis et al. (2012b), however, show less stiffness degradation despite using comparable rubber content. Their use of granular rubber (SR ≈ 1) and appears to have produced a more homogeneous and stable contact network that resists early nonlinearity. The more gradual reduction in G/G_0 in their study likely reflects the limited angularity and lower interparticle friction of the granulated material.

Figures 5a and 5b illustrate the evolution of damping ratio (ξ) with increasing shear strain for rubber contents of $\chi = 10\%$ and $\chi = 30\%$, respectively. At $\chi = 10\%$, the damping behaviour shows considerable variability across the literature, due largely to differences in rubber particle morphology and SR. Damping ratio at $\gamma = 0.0001\%$ in this study are in agreement with prior results from Feng and Sutter (2000), Anastasiadis et al. (2012b), Kaneko et al. (2013), and Pistolas et al. (2018), all of which used confining pressures in the 69–100 kPa range.

However, beyond $\gamma \approx 0.02\%$, the damping in 10ShRSm mixtures increases more sharply, reaching peak values of $\xi \approx 25$–27% around $\gamma = 0.1$–0.2%, which exceed those in all other compared studies. This accelerated rise in ξ is consistent with the early onset of stiffness degradation observed in Figure 4a. Compared to the more uniform, granular rubber used by Nakhaei et al. (2012) (SR ≈ 1), or the tyre chips used by Kaneko et al. (2013) (SR ≈ 2), ShR adopted in this study enhances frictional interaction within the soil matrix, promoting energy dissipation even

at medium strain levels. In the present study, ShR particles exhibit not only a high aspect ratio and angularity, but also visible fissures and surface cracks (Figure 1). Under cyclic loading, these fissures can deform, compress, and recover, absorbing part of the input energy and facilitating enhanced damping capacity, as demonstrated via x-ray tomographic tests in Fonseca et al. (2019). Additionally, the presence of cracks may reduce the effective stiffness at rubber-sand contacts, encouraging slippage and rearrangement, thereby amplifying the observed damping response at strain amplitudes beyond $\gamma \approx 0.02\%$. Similar damping behaviour was reported by Madhusudhan et al. (2019) for mixtures with high rubber content and large tyre shreds. The limiting shear strain (γ_{lim}) in 10ShRSm occurs at lower strain amplitudes than in the referenced studies, particularly those of Kaneko et al. (2013) and Pistolas et al. (2018), indicating that the mixture transitions to a peak earlier. This effect is attributed to the higher angularity and lower stiffness of ShR, which leads to greater relative motion between particles and earlier activation of damping mechanisms.

In Figure 5b, for $\chi = 30\%$, the damping behaviour falls within the envelope of previous studies, paralleling the trends observed for G/G_0 in Figure 4b. Compared to the $\chi = 10\%$ case, the absolute damping values are slightly reduced, particularly in the medium strain range. This observation is consistent with findings by Ehsani et al. (2015) and Li et al. (2016), who noted that damping increases with rubber content up to an optimal threshold (typically $\chi \approx 10$–15%) but may decline at higher rubber contents due to the development of a more homogeneous rubber phase and the reduction in interparticle sliding resistance. Despite not reaching γ_{lim} in most referenced studies, the upward trend in ξ beyond $\gamma \approx 0.5\%$ suggests that larger strain amplitudes ($\gamma > 1\%$) could yield further increases in damping, particularly in mixtures with highly deformable rubber content. This behaviour supports the hypothesis that rubber-like soils undergo progressive reorganisation at high strain, leading to more linear and dissipative behaviour dominated by rubber-to-rubber interactions.

The enhancement in damping is thus more pronounced in mixtures with elongated or high A_r rubber (e.g., ShR in this study; tyre chips in Kaneko et al., 2013) and in systems where SR > 1, i.e., rubber mean particle size larger than sand. At lower confining pressures, such as those used here ($\sigma'_m = 100$ kPa), the benefits of increased rubber content are most evident in mixtures where the sand skeleton maintains structural rigidity ($D_r \geq 65\%$) and the rubber phase contributes primarily to energy absorption. Conversely, studies using larger sand particles (SR < 1) or uniformly rounded rubber particles often report more moderate increases in damping, especially at small-to-intermediate strains (e.g., Nakhaei et al., 2012; Anastasiadis et al., 2012b).

3.2 Cyclic effect on stiffness and damping properties of ShRSm

This study examines the evolution of stiffness, damping capacity, and liquefaction susceptibility in ShRSm with varying rubber content, and strain amplitude ($\gamma = 0.1\%$ - 1%). The results in Figures 3, 4 and 5 show the typical dynamic behaviour of soils and RSm in initial loading cycles (N = 2 - 10), commonly used for geotechnical predictions, simulations and design. However, this provides an incomplete representation of dynamic behaviour, especially for changes in stiffness and damping over multiple cycles under strong motions and their aftermath. This investigation distinguishes thus between short-term and long-term (up to N = 400) cyclic loading regimes.

Bernal-Sanchez, J., McDougall, J., Barreto, D., Dimitriadi, V., Leak, J., & Anbazhagan, P. (2025). Influence of rubber content and particle morphology on the dynamic behaviour, liquefaction susceptibility and internal stability of shredded rubber-sand mixtures. *Geosynthetics International*, 1-21. Advance online publication. https://doi.org/10.1680/jgein.24.00157. For the purpose of open access, a CC BY 4.0 licence has been applied.

452 At low-medium strains (γ = 0.1%), LBS stiffness decreases from G = 19.2 MPa to G = 14 MPa after 20 cycles.
453 The evolution of G in LBS at high cycle counts contrasts with its minimal stiffness change observed after the
454 initial 10 cycles, where the specimen maintained its structural integrity without significant degradation. However,
455 at higher cycles, the progressive increase in PWP leads to a reduction in effective stress, causing the loss of
456 interparticle contacts and a subsequent decrease in stiffness. Figure 6a shows a gradual decrease in G of LBS after
457 130 cycles, leading to liquefaction as illustrated in the accumulation of r_u in Fig. 6c.

458 For χ = 10%, the rate of stiffness degradation remains relatively low, while for χ = 20–30%, the reduction in G is
459 almost negligible (Fig. 6a). This is attributed to the limited accumulation of PWP (shown in Fig 6c), which
460 preserves interparticle interactions and maintain soil rigidity under cyclic loading. Adding 10% rubber to LBS
461 shifts its behaviour from plastic to elastoplastic, and nearly elastic at higher rubber contents (χ > 10%) as explained
462 in depth with the use of stress paths in Bernal-Sanchez (2020). At γ = 0.2 and 1% (Figs. 6d-g), a substantial drop
463 in G is observed in LBS and 10ShRSm, with the minimum stiffness recorded just before liquefaction (Figs. 6f-i).
464 Although LBS begins with greater initial stiffness, its modulus declines more rapidly due to higher PWP.

465 Damping capacity (ξ) decreases uniformly across different rubber percentages until N = 20 (Fig. 6b), then
466 continues to decrease at a slower rate. LBS damping is marginally influenced by the cycle count until N = 10,
467 then gradually increases until N = 100. This suggests that friction damping in LBS may exceed the combined
468 effects of particle sliding and rubber deformation in ShRSm. Estimating ξ evolution in mineral soils and ShRSm
469 at medium-to-large strains remains however challenging and rather complex to predict in the long-term regime as
470 observed in Figs. 6b-e-h. While LBS damping rapidly decays due to loss of interparticle friction with PWP build-
471 up (Fig. 6c), ShRSm maintains sustained stiffness and damping degradation up to 400 cycles attributed to a lower
472 accumulation of PWP and r_u.

473 At γ = 0.2–1% (Fig. 6e–h), the benefits of ShRSm become more apparent. While LBS shows higher ξ at γ = 0.1%
474 during early cycles (Fig. 6b), mixtures with ShR achieve greater damping beyond 20 cycles, particularly at $\gamma \geq$
475 0.2%. This reflects the limited capacity of LBS for sustained frictional damping once particle rearrangement
476 stabilises, compared with the continued recoverable deformation of rubber in ShRSm. As a result, damping in
477 ShRSm is increasingly governed by the mechanical behaviour of rubber, with rubber-like characteristics becoming
478 dominant at $\chi \geq$ 10%.

479 ShRSm benefits from the compressibility and deformability of the small, shredded particles under cyclic loading.
480 X-ray microtomography on ShRSm (Fonseca et al., 2019) showed a small, reversible reduction of the rubber-
481 phase volume during loading with near recovery on unloading, alongside a persistent increase in sand–rubber
482 contact area. This behaviour reduces interparticle slippage and reinforces shear resistance. Since bulk rubber is
483 nominally incompressible, the observed volume change may be attributed to the opening and closure of cavities,
484 fissures and micro-cracks. The ShR used in this study exhibits such surface features (Fig. 1c–d), which act as
485 micro-deformation zones that accommodate strain and dissipate energy. These features allow the particles to bend,
486 compress and recover without structural failure, supporting a sustained mechanical response of ShRSm across

cycles and enhancing damping by distributing deformation within the rubber volume rather than confining dissipation solely to contact interfaces.

This long-term performance is consistent with mechanical stabilisation through void filling and the formation of persistent contact zones, as noted by Platzer et al. (2018) and Fonseca et al. (2019). The inclusion of rubber also reduces particle crushing (Fu et al., 2014), preserving the integrity of the sand skeleton while enabling recoverable deformation.

Alternatively, studies on the mechanics of polymer materials further demonstrate that the growth of cracks and cavities increases dissipated energy per cycle and alters loss parameters (Marco et al., 2017; Le Saux et al., 2010; Han et al., 2019). Cavitation and interfacial debonding in filled rubbers are also recognised as sources of volume change under cyclic loading (Le Cam et al., review; Federico et al., 2021; Yakovlev et al., 2025). These observations are consistent with the behaviour of ShR: the surface fissures and cavities identified in this study provide sites where local opening, closure, and shear can occur, generating volumetric strains that supplement conventional viscoelastic hysteresis. In practice, this means that ShRSm do not rely solely on interparticle friction to dissipate energy, but also benefit from localised defect deformation within the rubber phase itself. This dual mechanism helps to explain why damping in ShRSm not only persists but often increases with cycling, when LBS stabilises or decreases. The implication is that fissures are not merely imperfections but functional microstructural features that contribute to longer term resilience by enabling distributed energy dissipation across the rubber volume, supporting the sustained damping performance observed at $\chi \geq 10\%$ and $\gamma \geq 0.2\%$.

ShRSm dynamic response contrasts with other studies in the literature that explored RSm under different testing conditions and particle configurations. For instance, Madhusudhan (2019) tested dry mixtures containing coarse tyre shreds with high A_r, reporting no significant damping degradation, even under large cyclic strains. The absence of PWP and the high deformability of large rubber particles likely contributed to this behaviour. In contrast, Mashiri et al. (2016) performed undrained cyclic triaxial tests on saturated sand - tyre chip mixtures and reported a notable reduction in stiffness and damping within the first 15 cycles. Their study used poorly graded sand (D_{50} = 0.35 mm) and rectangular chips (6 × 18 mm) at SR > 15 and observed that degradation was closely associated with PWP build-up and loss of contact forces. Compared to these studies, ShRSm in this investigation, with SR ≈ 1.88 and embedded in a medium-dense sand matrix, demonstrate intermediate behaviour: while some degradation is observed in the early cycles, ShRSm maintains internal stability and sustained damping capacity over a longer cyclic regime.

The aforementioned differences highlight the combined effects of rubber-to-sand SR, morphology, and saturation, all of which influence the extent of particle rearrangement, contact stability, and ultimately, the cyclic performance of RSm. The cyclic resilience of ShRSm under medium-to-large strains is therefore demonstrated through three critical performance indicators: reduced stiffness degradation, delayed PWP accumulation, and sustained damping capacity with respect to the sand-only (i.e. stiff) mixtures. These characteristics are especially relevant for GSI systems, such a retrofitted RSm foundations, where the ability of the modified geomaterial to deform, recover, and dissipate energy across multiple seismic cycles is essential for protecting the overlying structure integrity.

Bernal-Sanchez, J., McDougall, J., Barreto, D., Dimitriadi, V., Leak, J., & Anbazhagan, P. (2025). Influence of rubber content and particle morphology on the dynamic behaviour, liquefaction susceptibility and internal stability of shredded rubber-sand mixtures. *Geosynthetics International*, 1-21. Advance online publication. https://doi.org/10.1680/jgein.24.00157. For the purpose of open access, a CC BY 4.0 licence has been applied.

3.3 Internal stability, liquefaction phenomena and stiffness / damping degradation in ShRSm

The internal stability criterion using normalised entropy coordinates, based on the PSD of a granular material (Lőrincz, 1986), is here adapted to predict the liquefaction susceptibility of rubber-containing mixtures (Fig. 7). According to Bernal-Sanchez et al. (2023), all sand only specimen are found in the unstable zone, with normalised base entropy (A) lower than 0.6. All these samples are characterised for being better graded than the rubber only samples (i.e. higher B) but having smaller average grain sizes and hence lower A-coordinates. All these studies reported that sand soils eventually liquefed due to the accumulation of PWP. Bernal-Sanchez et al. (2023) demonstrated that lower PWP accumulation and reduced liquefaction susceptibility in RSm, consistent with previous studies (Kaneko et al., 2013; Otsubo et al., 2016; Bahadori and Roohollah, 2018; Enquan and Qiong, 2019; Bernal-Sanchez et al., 2020; Amuthan et al., 2020; Rios et al., 2021), are directly linked to soil gradation. In the stable zone, rubber-only specimens and RSm with a normalised base entropy (A) greater than 0.6, characterised by larger average grain sizes, exhibited no liquefaction and significantly lower liquefaction potential. This aligns with findings by Barreto and Imre (2018), who noted that larger particles bear more stress. Although these mixtures also fall within the suffusion zone, rubber's ability to deform and change volume under large stresses prevents particle detachment. The high interparticle friction allows rubber particles to remain attached to surrounding grains, effectively locking contacts and minimising sliding. Consequently, suffusion of rubber particles is unlikely, as the rubber matrix maintains particle cohesion. This suggests that, for soft-rigid mixtures such as RSm, the suffusion zone may function as an extension of the stable zone, rather than an area of particle migration.

Conversely, other studies (Promputthangkoon and Hyde, 2008; Shariatmadari et al., 2018) show increased liquefaction susceptibility with added rubber. Smaller rubber particles may also lower the normalised base entropy below 0.6 (left on Fig. 7), creating an internally unstable matrix that leads to liquefaction as occurred in the aforementioned papers. The smaller average grain size in all mineral soils in Fig. 7 explains their higher susceptibility to liquefy under external loading, as demonstrated in this study (Fig. 6).

However, Lőrincz's (1986) stability criterion considers PSD but not other sample characteristics (e.g., density, particle shape, stiffness, inter-particle friction, mineralogy) or test conditions (e.g., strain level, or prolonged cyclic effect). One factor clearly affecting the liquefaction resistance of sands and RSm is the accumulation of deformation, as observed in Figs. 6c, f, i. Following Tsuha et al. (2012), who categorised driven pile behaviour into stable, unstable, and meta-stable states in offshore foundations, this study identifies two behaviours under cyclic loading (see in Fig. 8a) in undrained saturated conditions:

(i) stable, where PWP stabilises or accumulates slowly, and the specimen does not liquefy;

(ii) unstable, where PWP rapidly increases, reaching $r_u > 0.9$, and the specimen eventually liquefies.

Figure 8a presents the last recorded value of the excess pore pressure ratio r_u, either at the point of liquefaction for sand-like soils or at N = 400 for rubber-like soils that remained stable. The accumulation of PWP progressively weakens inter-particle forces, leading to a reduction in effective stress and, consequently, a loss of soil strength

(Wichtmann and Triantafyllidis, 2016; Zhang et al., 2016). This phenomenon is particularly pronounced in sand-only specimens, where PWP increases rapidly under cyclic loading, causing r_u to exceed 0.9 within 15, 40, and 130 cycles for shear strains of 0.1%, 0.2%, and 1%, respectively. Such rapid PWP accumulation accelerates soil liquefaction, placing sand within the unstable zone.

In contrast, mixtures containing ShR exhibit a significantly lower accumulation of PWP, thereby enhancing their liquefaction resistance. Figures 6c, 8a illustrate that as rubber content increases, the rate of PWP buildup slows, delaying or even preventing the occurrence of $r_u = 1$. This effect is attributed to the higher compressibility and deformability of rubber particles, which provide a temporary volume-change mechanism (Fonseca et al., 2019) that reduces the rate at which PWP develops under undrained conditions. The influence of rubber inclusion is most pronounced at χ = 20-30%, where specimens withstand up to 400 cycles without liquefying, even at high strain levels. However, at larger strains, the effectiveness of rubber in mitigating PWP build-up diminishes slightly due to increased particle rearrangement and the eventual saturation of energy dissipation mechanisms. Yet, the results confirm that higher rubber contents consistently enhance the long-term stability of RSm under cyclic loading by delaying or completely preventing liquefaction, reinforcing their suitability for GSI applications.

Bernal-Sanchez et al. (2023) recommended the addition of at least 10% rubber, with a normalised base entropy A > 0.6 exhibited by specimens with larger particles, to enhance the liquefaction resistance of mineral soils. The results shown in Fig. 6c, f, i, and 8a show that while this is true in the initial cycles, even mixtures containing 10% rubber may eventually liquefy after 80-295 cycles at 0.2% and 1% strains, respectively. Thus, the latter experimental results shown in this study demonstrate that the cyclic effect should also be considered at medium-to-large strains under saturated conditons. The internal stability criterion proposed by Bernal-Sanchez et al. (2023) remains yet suitable for higher rubber contents (χ > 10%) at 1% strains.

Figure 8b shows the evolution of the normalised shear modulus (G/G_0) with the number of cycles at medium-to-large strain amplitudes, with the final recorded value (shown in parenthesis) corresponding either to liquefaction or to N = 400. Compared with Fig. 3b, which illustrates stiffness degradation at a fixed cycle (N = 2), Fig. 8b highlights the progressive loss of stiffness over time. The results indicate that stiffness degradation is more pronounced in sand-like mixtures (χ = 0, 10%), which reach liquefaction when G/G_0 falls below about 0.3. For instance, 10ShRSm crosses this threshold after 80 cycles at γ = 0.2% and after 295 cycles at γ = 1%. In contrast, mixtures with $\chi \geq 20\%$ maintain $G/G_0 > 0.3$ throughout, showing improved resilience under cyclic loading.

Figure 8c presents the variation in damping ratio (ξ) with rubber content for different strain amplitudes and selected cycle numbers. At small strain amplitudes (γ = 0.05–0.1%), damping initially increases with rubber addition but peaks at χ = 10% before declining, with higher rubber contents (χ = 20–30%) showing greater ξ degradation over cycles. At larger strain amplitudes (γ = 0.2–1%), however, the trend reverses: mixtures with χ = 20–30% exhibit more stable damping behaviour over long cycles, while LBS and χ = 10% suffer faster reductions. At γ = 1%, ShRSm achieves higher ξ values than LBS, confirming the improved energy dissipation capacity of ShRSm under large cyclic strains.

Bernal-Sanchez, J., McDougall, J., Barreto, D., Dimitriadi, V., Leak, J., & Anbazhagan, P. (2025). Influence of rubber content and particle morphology on the dynamic behaviour, liquefaction susceptibility and internal stability of shredded rubber-sand mixtures. *Geosynthetics International*, 1-21. Advance online publication. https://doi.org/10.1680/jgein.24.00157. For the purpose of open access, a CC BY 4.0 licence has been applied.

593 Table 4 complements these observations by providing quantitative values for stiffness and damping degradation
594 at N = 20, 100 and 400 cycles. At γ = 0.1%, LBS lost around 28% of its initial stiffness after 20 cycles and
595 liquefied before 400, while χ = 20–30% mixtures lost less than 15% even after 400 cycles. Damping behaviour at
596 this strain level differed, with LBS and χ = 10% showing smaller ξ reductions, up to 40% by N = 400, than χ =
597 20–30%, with around 50% loss by N = 400. At higher strain amplitudes (γ = 0.2%), stiffness degradation was
598 much greater in LBS and χ = 10%, with 75% and 37% losses respectively by N = 20, whereas χ = 20–30% mixtures
599 retained stiffness, with less than 14% loss, and showed smaller damping reductions over 400 cycles.

600 The findings from this study (Figs. 8b, c) show thus that G and ξ for both LBS and ShRSm are notably affected
601 by cyclic loading at medium-to-large strains, contrary to other studies where no degradation was reported when
602 tested under dry conditions (Kokusho, 1980; Nakhaei et al., 2012; Madhusudhan et al., 2019). Overall, these
603 results highlight that increasing rubber content delays stiffness degradation and sustains damping capacity under
604 large strain cycles, while the influence on damping degradation is more complex at very small strains.

605 The stability of RSm under cyclic loading is thus governed by the interaction mechanisms between rubber and
606 sand particles, which influence the material's stiffness evolution, pore pressure response, and liquefaction
607 resistance. At low rubber contents (χ = 10%), the mixture retains a sand-like behaviour, where rigid sand-to-sand
608 contacts dominate. Rubber primarily acts as a void filler, providing some additional flexibility but not significantly
609 altering the stress transfer mechanisms between mineral grains. As rubber content increases ($\chi \geq$ 20%), the mixture
610 transitions toward a rubber-like behaviour, where direct grain contacts are reduced, and rubber-to-rubber and
611 rubber-to-sand interactions become dominant. This results in a more uniform stress distribution that prevents
612 localised strain concentrations. Under cyclic loading, ShR appear to compress and recover, modifying the contact
613 forces between grains and reducing the likelihood of particle slippage. This behaviour enhances energy dissipation
614 (Fonseca et al., 2019) and limits excess PWP buildup, thereby increasing the number of cycles required for
615 liquefaction, as observed in Figures 6 and 8. Furthermore, the high interparticle friction of rubber (μ = 1) compared
616 to sand (μ = 0.24) (Lopera Perez et al., 2016) reduces internal collapse, delaying stiffness degradation and
617 improving long-term resilience against cyclic loading. In addition, the fissures and cavities present in ShR may
618 provide local sites for volumetric strain and recoverable deformation (Federico et al., 2021; Yakovlev et al., 2025).
619 As the mixture shifts from sand-like to rubber-like behaviour, dissipation mechanisms therefore move from purely
620 frictional slip at rigid contacts to rubber deformation and enhanced hysteresis, as seen in the literature with other
621 polymers (Marco et al., 2017; Le Saux et al., 2010; Han et al., 2019). This dual contribution of recoverable
622 deformation and increased energy loss may explain both the higher damping ratios at $\gamma \geq$ 0.2% and the improved
623 resistance to liquefaction, confirming that the enhanced cyclic stability of ShRSm.

624 The findings of this study have meaningful implications for the design and implementation of GSI systems. The
625 inclusion of ShR in sand, particularly at contents of 20–30%, enhances thus the long-term resilience of the
626 composite material under cyclic loading. This is especially valuable for scenarios involving high-cycle dynamic
627 events such as prolonged aftershocks (Nazari et al., 2014) or repeated loading from transport infrastructure
628 (Murillo et al., 2009; Signes et al., 2017). Although increased rubber content is associated with a reduction in

shear modulus, this trade-off is counterbalanced by enhanced damping capacity and reduced pore pressure build-up. At rubber contents of $\chi = 30\%$, damping remains stable over long-term loading, and liquefaction resistance is significantly improved under high strain amplitudes. These benefits are would be particularly advantageous in non load-bearing GSI applications such as peripheral wave barriers, where lower stiffness relative to the surrounding soil promotes wave scattering and energy dissipation (Mahdavisefat, 2018; Toygar et al. 2024; Bernal-Sanchez et al., 2024).

Recent large-scale field testing by Vratsikidis and Pitilakis (2022) further supports these findings, demonstrating that gravel–rubber mixtures with at least 30% rubber by mass attenuated accelerations more effectively than lower-rubber-content alternatives, even when placed directly beneath a structure. This indicates that reduced stiffness does not necessarily compromise seismic isolation performance, provided the system is correctly configured. Moreover, the observed increase in damping ratio at small-to-medium strain levels promotes period elongation, reducing the risk of resonance by shifting the natural frequency of the soil-structure system away from dominant seismic frequencies (Tsang and Pitilakis, 2019; Pitilakis et al., 2021; Bernal-Sanchez, 2022, 2024). These findings highlight thus the suitability of ShRSm not only as resilient materials but also as functionally adaptive components of seismic protection systems.

4 SUMMARY AND CONCLUSIONS

This study has examined the dynamic behaviour, liquefaction susceptibility, and internal stability of ShRSm under cyclic loading, focusing on how variations in rubber content, particle shape, and size ratio affect their resilience. The findings provide several conclusions, some of which reinforce previous work while others provide new insights into the long-term performance of rubber-soil mixtures under cyclic loading.

- At small strain levels ($\gamma \leq 0.1\%$), the expected increase in damping ratio (ξ) and decrease in shear modulus (G) with rubber content were confirmed. This is consistent with earlier findings (e.g., Feng & Sutter, 2000; Anastasiadis et al., 2012b), and attributed to the frictional effects and deformability of rubber particles.
- By comparing this study with the literature, it was found that the size and shape of rubber particles strongly influence the evolution of stiffness and damping in RSm at medium-to-large strains. Larger particles (SR > 1) or elongated particles (Ar > 1) promote greater stiffness degradation but also enhance damping, as increased sand-to-sand contacts concentrate strain while allowing more deformation of the ShR particles. The angular and elongated ShR used here (Ar = 2–6), together with the presence of surface fissures and cracks, led to an earlier onset of stiffness degradation in mixtures with $\chi = 10\%$. These micro-defects act as local deformation zones that lead to an overall higher damping. At $\chi = 30\%$, however, the influence of particle geometry becomes less pronounced, as rubber-like behaviour dominates and damping characteristics converge toward a more uniform response across mixtures.A key contribution of this study is the long-term evaluation of cyclic loading (N = 400). The results reveal that ShRSm maintains stiffness and damping more effectively than sand-only mixtures, particularly at $\gamma = 0.2\%$ and 1%, highlighting their resilience under prolonged dynamic excitation. This demonstrates a material-level definition of resilience, expanding upon short-term dynamic tests in earlier works.

- The inclusion of at least 10% ShR improved liquefaction resistance through reduced PWP build-up and more stable stiffness degradation. However, mixtures with χ = 10% still liquefied under high strain amplitudes and longer cycles, suggesting that a threshold of 20% rubber content is necessary to fully exploit the liquefaction mitigation benefits under stronger loading regimes.
- The internal stability of ShRSm is enhanced with higher rubber content. Both LBS and ShRSm become unstable when $G/G_0 < 0.3$. However, adding at least 20% ShR mitigates this reduction, enhancing the internal stability of ShRSm and prolonging its resilience against sustained dynamic loading up to 1% strain.

This study highlights the potential of ShRSm as a sustainable and effective material for improving the seismic performance of retrofitted soils. Incorporating at least 10-20% ShR in mineral soils can mitigate the degradation in stiffness and damping capacity, particularly under saturated conditions and high cycle counts. This can be beneficial in scenarios involving strong motions and their aftermath or intense ground vibrations, such as those from traffic. While this study primarily focuses on mixtures with specific PSD and SR, future research will investigate the influence of more realistic soil gradations on RSm behaviour under dynamic loading. Additionally, further resonant column and cyclic triaxial tests will assess the effects of a wider range of confining pressures and relative densities, providing deeper insights into the macro-scale performance of ShRSm in seismic applications.

ACKNOWLEDGMENTS

The authors extend their gratitude to all contributors who supported this research in various forms. Special thanks are owed to W. Laing for his indispensable assistance and patience throughout the experimental testing phase. The authors would also like to thank Edinburgh Napier University for the provision of resources essential for the execution of such complex and advanced experimental testing. This work would not have been possible without the strong collaboration within the Geomechanics Micro to Macro research group (GM2M) whose insights and support were fundamental in advancing this research.

NOTATIONS

All units are presented in SI base units, as per journal guidelines.

A_r = Aspect ratio of rubber particles

CSR = Cyclic stress ratio

D_r = Relative density (kg/m^3)

D_{50} = Median particle diameter (m)

e_0 = Initial void ratio

f = Frequency (Hz or s^{-1})

G = Shear modulus (Pa)

Bernal-Sanchez, J., McDougall, J., Barreto, D., Dimitriadi, V., Leak, J., & Anbazhagan, P. (2025). Influence of rubber content and particle morphology on the dynamic behaviour, liquefaction susceptibility and internal stability of shredded rubber-sand mixtures. *Geosynthetics International*, 1-21. Advance online publication. https://doi.org/10.1680/jgein.24.00157. For the purpose of open access, a CC BY 4.0 licence has been applied.

G/G_0 = Normalised shear modulus

G_0 = Initial shear modulus at small strains (Pa)

γ = Shear strain

γ_a = Shear strain amplitude

γ_{lim} = Limiting shear strain for onset of nonlinearity

N = Number of loading cycles

r_u = Excess pore pressure ratio

PWP = Pore Water Pressure (Pa)

Δu = Increase in PWP (Pa)

SR = Particle size ratio, D_{R50} / D_{S50}

ξ = Damping ratio

χ = Rubber content by weight

σ_m = Mean confining stress (Pa)

σ'_m = Mean effective confining stress (Pa)

ABBREVIATIONS

CT	Cyclic Triaxial
LBS	Leighton Buzzard sand
LQ	Liquified
GSI	Geotechnical Seismic Isolation
PSD	Particle Size Distribution
RC	Resonant Column
RSm	Rubber-Soil mixtures
ShR	Shredded Rubber
ShRSm	Shredded Rubber-Sand mixtures
TDA	Tyre Derived Aggregate

REFERENCES

Bernal-Sanchez, J., McDougall, J., Barreto, D., Dimitriadi, V., Leak, J., & Anbazhagan, P. (2025). Influence of rubber content and particle morphology on the dynamic behaviour, liquefaction susceptibility and internal stability of shredded rubber-sand mixtures. *Geosynthetics International*, 1-21. Advance online publication. https://doi.org/10.1680/jgein.24.00157. For the purpose of open access, a CC BY 4.0 licence has been applied.

Amuthan, M.S., Boominathan, A. and Banerjee, S. (2020). Undrained cyclic responses of granulated rubber-sand mixtures. *Soils and Foundations*, 60, pp. 871–885. DOI: 10.1016/j.sandf.2020.06.007

Anastasiadis, A., Senetakis, K. and Pitilakis, K. (2012a). Small-strain shear modulus and damping ratio of sand-rubber and gravel-rubber mixtures. *Geotechnical and Geological Engineering*, 30(2), pp. 363–382. DOI: 10.1007/s10706-011-9473-2.

Anastasiadis, A., Senetakis, K., Pitilakis, K., Gargala, C., Karakasi, I., Edil, T. and Dean, S.W. (2012b). Dynamic behaviour of sand/rubber mixtures. Part I: Effect of rubber content and duration of confinement on small-strain shear modulus and damping ratio. *Journal of ASTM International*, 9(2). DOI: 10.1520/JAI103680.

ASTM D3999-11. Standard test methods for the determination of the modulus and damping properties of soils using the cyclic triaxial apparatus. ASTM International, West Conshohocken.

ASTM D4015-15. Standard test methods for modulus and damping of soils by fixed-base resonant column devices. ASTM International, West Conshohocken.

ASTM D854-14. Standard Test Methods for Specific Gravity of Soil Solids by Water Pycnometer. In: ASTM International Standard Methods.

ASTM D7181-11. Standard test method for consolidated drained triaxial compression test for soils. ASTM International Standard Method.

ASTM D7382-08. Standard test methods for determination of maximum dry unit weight and water content range for effective compaction of granular soils using a vibratory hammer. ASTM International Standard Method.

ASTM D6270-12. Standard practice for use of scrap tires in civil engineering applications.

ASTM D698-12e2, Standard Test Methods for Laboratory Compaction Characteristics of Soil Using Standard Effort.

BS 1377-4 (1990). Methods of test for soils for civil engineering purposes - Part 4: compaction-related tests. British Standards Institution, London.

Barreto, D. and Imre, E. (2018). Grading entropy coordinates and shear stiffness in granular materials. *IS Atlanta 2018 Paper Abstracts: Particles/Crushing II.*

Bahadori, H. and Farzalizadeh, R. (2018). Dynamic properties of saturated sands mixed with tyre powders and tyre shreds. *International Journal of Civil Engineering*, 16(4), pp. 395–408. DOI: 10.1007/s40999-016-0136-9.

Bahadori, H. and Manafi, S. (2015). Effect of tyre chips on dynamic properties of saturated sands. *International Journal of Physical Modelling in Geotechnics*, 15(3), pp. 116–128. DOI: 10.1680/ijpmg.13.00014.

Bernal-Sanchez, J., McDougall, J., Barreto, D., Dimitriadi, V., Leak, J., & Anbazhagan, P. (2025). Influence of rubber content and particle morphology on the dynamic behaviour, liquefaction susceptibility and internal stability of shredded rubber-sand mixtures. *Geosynthetics International*, 1-21. Advance online publication. https://doi.org/10.1680/jgein.24.00157. For the purpose of open access, a CC BY 4.0 licence has been applied.

Banzibaganye, G. and Vrettos, C. (2022). Resonant column tests on mixtures of different sands with coarse tyre rubber chips. *Geotechnical and Geological Engineering*, 40(6), pp. 5725–5738. DOI: 10.1007/s10706-022-02244-0.

Bernal-Sanchez, J., McDougall, J., Barreto, D., Miranda, M. and Marinelli, A. (2018). Dynamic behaviour of shredded rubber soil mixtures. *16th European Conference on Earthquake Engineering*, Thessaloniki.

Bernal-Sanchez, J. (2020). Cyclic performance on rubber-soil mixtures to enhance seismic protection. Dissertation, Edinburgh Napier University.

Bernal-Sanchez, J., McDougall, J., Miranda, M. and Barreto, D. (2022). Dynamic behaviour of a geotechnical seismic isolation system with rubber-sand mixtures to enhance seismic protection. *3rd European Conference on Earthquake Engineering & Seismology.*

Bernal-Sanchez, J., Leak, J. and Barreto, D. (2023). Rubber-soil mixtures: use of grading entropy theory to evaluate stiffness and liquefaction susceptibility. *Bulletin of Earthquake Engineering*, 21, pp. 3777–3796. DOI: 10.1007/s10518-023-01673-3.

Bernal-Sanchez, J., Mcdougall, J., Barreto, D., Dimitriadi, V., Leak, J. and Nseabasi, M. (2024). An innovative approach to geotechnical seismic isolation: rubber-soil mixture trenches. *18th World Conference on Earthquake Engineering*.

Boulanger, R.W. and Idriss, I.M. (2014). CPT and SPT based liquefaction triggering procedures. Report No. UCD/CGM-14/01. Davis, CA: Center for Geotechnical Modeling, University of California.

Consoli, N., Casagrande, M., Thomé, A., Rosa, F. D., & Fahey, M. (2009). Effect of relative density on plate loading tests on fibre-reinforced sand. *Geotechnique, 59*, pp. 471-476.

Dushmantha, A., Jayakody, S., Gui, Y. and Gallage, C. (2025). A comprehensive review of the resilient behaviour of unbound granular pavement materials. *Journal of Traffic and Transportation Engineering*, 12(3), pp. 522–550. DOI: 10.1016/j.jtte.2024.06.004

Edil, T.B. and Bosscher, P.J. (1994). Engineering properties of tire chips and soil mixtures. *Geotechnical Testing Journal*, 17(4), pp. 453. DOI: 10.1520/GTJ10306J

Edincliler, A., Baykal, G. and Saygılı, A. (2010). Influence of different processing techniques on the mechanical properties of used tires in embankment construction. *Waste Management*, 30, pp. 1073–1080. DOI: 10.1016/j.wasman.2009.09.031

Ehsani, M., Shariatmadari, N. and Mirhosseini, S.M. (2015). Shear modulus and damping ratio of sand-granulated rubber mixtures. *Journal of Central South University*, 22, pp. 3159–3167. DOI: 10.1007/s11771-015-2853-7.

El Shamy, U. and Denissen, C. (2012). Microscale energy dissipation mechanisms in cyclically-loaded granular soils. *Geotechnical and Geological Engineering*, 30(2), pp. 343–361. DOI: 10.1007/s10706-011-9472-3.

Bernal-Sanchez, J., McDougall, J., Barreto, D., Dimitriadi, V., Leak, J., & Anbazhagan, P. (2025). Influence of rubber content and particle morphology on the dynamic behaviour, liquefaction susceptibility and internal stability of shredded rubber-sand mixtures. *Geosynthetics International*, 1-21. Advance online publication. https://doi.org/10.1680/jgein.24.00157. For the purpose of open access, a CC BY 4.0 licence has been applied.

783 Enquan, Z. and Qiong, W. (2019). Experimental investigation on shear strength and liquefaction potential of
784 rubber-sand mixtures. *Advances in Civil Engineering*. DOI: 10.1155/2019/5934961.

785 ETRMA (2015). End-of-life tyre report 2015. Accessed in: ttps://www.etrma.org/wp-
786 content/uploads/2019/09/elt-report-v9a-final.pdf

787 Fiamingo, A., Chiaro, G., Murali, A. and Massimino, M. R. (2025a). Geotechnical characterization of soil–rubber
788 mixtures with well-graded gravel. *Geosynthetics International*. DOI: 10.1680/jgein.24.00177.

789 Fiamingo, A., Chiaro, G., Murali, A. and Massimino, M. R. (2025b). Response to discussion: Geotechnical
790 characterization of soil–rubber mixtures with well-graded gravel. *Geosynthetics International*. DOI:
791 10.1680/jgein.25.00039.

792 Fonseca, J., Bernal-Sanchez, J., Riaz, A., Barreto, D., McDougall, J., Miranda-Manzanares, M., Marinelli, A. and
793 Dimitriadi, V. (2019). Particle–scale interactions and energy dissipation mechanisms in sand–rubber mixtures.
794 *Géotechnique Letters*, 9(4), pp. 1–6. DOI: 10.1680/jgele.18.00221.

795 Fu, R., Coop, M.R. and Li, X.Q. (2017). Influence of particle type on the mechanics of sand–rubber mixtures.
796 *Journal of Geotechnical and Geoenvironmental Engineering*, 143(9). DOI: 10.1061/(ASCE)GT.1943-
797 5606.0001680.

798 Ghazavi, M. (2004). Shear strength characteristics of sand-mixed with granular rubber. *Geotechnical and*
799 *Geological Engineering*, 22(3), pp. 401–416. DOI: 10.1023/B.0000025035.74092.6c.

800 Guha-Sapir, D., Hoyois, P., Wallemacq, P. and Below, R. (2016). Annual disaster statistical review 2016 - The
801 numbers and trends. Centre for Research on the Epidemiology of Disasters (CRED). Accessed:
802 https://www.emdat.be/sites/default/files/adsr_2016.pdf

803 Han, Q., Zhang, L. and Wu, Y. (2019). Relationship between dynamic fatigue crack propagation properties and
804 viscoelasticity of natural rubber/silicone rubber composites. *RSC Advances*, 9(51), pp. 29813–29820. DOI:
805 10.1039/c9ra05833h

806 Hazarika, H., Kohama, E. and Sugano, T. (2008). Underwater shake table tests on waterfront structures
807 protected with tire chips cushion. *Journal of Geotechnical and Geoenvironmental Engineering*, 134(12), pp.
808 1706–1719. DOI: 10.1061/(ASCE)1090-0241(2008)134:12(1706).

809 Ishihara, K. (1996). *Soil behaviour in earthquake geotechnics*. Oxford University Press, Oxford.

810 Jensen, M. R. (2024). Estimating relative density from shallow depth CPTs in normally consolidated and
811 overconsolidated siliceous sand. *Canadian Geotechnical Journal.* DOI: 10.1139/cgj-2024-0136.

Bernal-Sanchez, J., McDougall, J., Barreto, D., Dimitriadi, V., Leak, J., & Anbazhagan, P. (2025). Influence of rubber content and particle morphology on the dynamic behaviour, liquefaction susceptibility and internal stability of shredded rubber-sand mixtures. *Geosynthetics International*, 1-21. Advance online publication. https://doi.org/10.1680/jgein.24.00157. For the purpose of open access, a CC BY 4.0 licence has been applied.

812 Kaneko, T., Orense, R.P., Hyodo, M. and Yoshimoto, N. (2013). Seismic response characteristics of saturated
813 sand deposits mixed with tire chips. *Journal of Geotechnical and Geoenvironmental Engineering*, 139(4), pp.
814 633–643. DOI: 10.1061/(ASCE)GT.1943-5606.0000752

815 Kelly, J. and Van Engelen, N. (2015). Fiber-reinforced elastomeric bearings for vibration isolation. *Journal of*
816 *Vibration and Acoustics*, 138.

817 Kim, H.K. and Santamarina, J.C. (2008). Sand-rubber mixtures (large rubber chips). *Canadian Geotechnical*
818 *Journal*, 45, pp. 1457-1466. DOI: 10.1139/T08-070

819 Kokusho, T. (1980). Cyclic triaxial test of dynamic soil properties for wide strain range. *Soils and Foundations*,
820 20, pp. 45–60. DOI: 10.3208/sandf1972.20.2_45

821 Kowalska, M. and Vrettos, C. (2024). Effect of layering and pre-loading on the dynamic properties of sand–
822 rubber specimens in resonant column tests. *Acta Geotechnica*, 20(2), pp. 607–624. DOI: 10.1007/s11440-024-
823 02398-6

824 Krogh L., Quinteros S., Engin H.K., and Lunne T. (2022). Revisiting interpretation of relative density from
825 shallow depth CPTs in sand. *Canadian Geotechnical Journal*. 59(6), pp. 808-826. https://doi.org/10.1139/cgj-
826 2021-0200

827 Kumar, S.S. and Krishna, A.M. (2013). Seismic ground response analysis of some typical sites of Guwahati
828 City. *International Journal of Geotechnical Earthquake Engineering*, 4, pp. 83–101. DOI:
829 10.4018/jgee.2013010106

830 Kumar, S.S., Krishna, A.M. and Dey, A. (2017). Evaluation of dynamic properties of sandy soil at high cyclic
831 strains. *Soil Dynamics and Earthquake Engineering*, 99, pp. 157–167. DOI: 10.1016/j.soildyn.2017.05.016.

832 Kramer, S.L. (1996). *Geotechnical earthquake engineering*. 1st ed. Upper Saddle River, NJ: Prentice-Hall.
833 ISBN 0-13-374943-6.

834 Le Saux, V., Marco, Y., Calloch, S., Doudard, C. and Charrier, P. (2010). Fast evaluation of the fatigue lifetime
835 of elastomers based on a heat build-up protocol. *International Journal of Fatigue*, 32(10), 1582–1590. DOI:
836 10.1016/j.ijfatigue.2010.02.015

837 Lee, J.S., Dodds, J. and Santamarina, J.C. (2007). Behaviour of rigid-soft particle mixtures. *Journal of Materials*
838 *in Civil Engineering*, 19(2), pp. 179–184. DOI: 10.1061/(ASCE)0899-1561(2007)19:2(179).

Bernal-Sanchez, J., McDougall, J., Barreto, D., Dimitriadi, V., Leak, J., & Anbazhagan, P. (2025). Influence of rubber content and particle morphology on the dynamic behaviour, liquefaction susceptibility and internal stability of shredded rubber-sand mixtures. *Geosynthetics International*, 1-21. Advance online publication. https://doi.org/10.1680/jgein.24.00157. For the purpose of open access, a CC BY 4.0 licence has been applied.

Lee, C., Truong, Q.G., Lee, W. and Lee, J.S. (2010). Characteristics of rubber-sand particle mixtures according to size ratio. *Journal of Materials in Civil Engineering*, 22(4), pp. 323–331. DOI: 10.1061/(ASCE)MT.1943-5533.0000027.

Li, B., Huang, M. and Zeng, X. (2016). Dynamic behaviour and liquefaction analysis of recycled-rubber sand mixtures. *Journal of Materials in Civil Engineering*, 28(11). DOI: 10.1061/(ASCE)MT.1943-5533.0001629.

Liu, F., Wang, J., Zhou, B., Wu, M., He, J., Bin, J. (2023). Shaking table study on rubber-sand mixture cored composite block as a low-cost isolation bearing for rural houses. *Journal of Building Engineering*, 76. DOI: 10.1016/j.jobe.2023.107413.

Lopera Perez, J.C., Kwok, C.Y. and Senetakis, K. (2016). Effect of rubber size on the behaviour of sand rubber mixtures: a numerical investigation. *Computers and Geotechnics*. DOI: 10.1016/j.compgeo.2016.07.005.

Look, B. G. (2007). *Handbook of geotechnical investigation and design tables*. Taylor & Francis.

Lőrincz, J. (1986). Grading entropy of soils. Dissertation, Technical University of Budapest (in Hungarian).

Madhusudhan, A., Boominathan, B.R. and Banerjee, S. (2019). Factors affecting strength and stiffness of dry sand-rubber tire shred mixtures. *Geotechnical and Geological Engineering*. DOI: 10.1007/s10706-018-00792-y.

Mahdavisefat, E., Salehzadeh, H., Heshmati, A.A. (2018). Full-scale experimental study on screening effectiveness of SRM-filled trench barriers. *Géotechnique*. 68(10), pp. 869–882.

Marco, Y., Huneau, B., Masquelier, I., Le Saux, V. and Charrier, P. (2017). Prediction of fatigue properties of natural rubber based on the descriptions of the cracks population and of the dissipated energy. *Polymer Testing*, 59, pp. 67–74. DOI: 10.1016/j.polymertesting.2017.01.015

Masad, E., Taha, R., Ho, C. and Papagiannakis, T. (1996). Engineering properties of tire/soil mixtures as a lightweight fill material. *Geotechnical Testing Journal*, 19(3), pp. 297–304. DOI: 10.1520/GTJ10355J.

Mashiri, M.S., Vinod, J.S. and Sheikh, M.N. (2016). Liquefaction potential and dynamic properties of sand-tyre chip mixtures. *Geotechnical Testing Journal*. DOI: 10.1520/GTJ20150031.

Molaei, M. and Fatemi, A. (2021). Fatigue performance of additive manufactured metals under variable amplitude service loading conditions including multiaxial stresses and notch effects: Experiments and modelling. *International Journal of Fatigue*, 145. DOI: 10.1016/j.ijfatigue.2020.106002

Bernal-Sanchez, J., McDougall, J., Barreto, D., Dimitriadi, V., Leak, J., & Anbazhagan, P. (2025). Influence of rubber content and particle morphology on the dynamic behaviour, liquefaction susceptibility and internal stability of shredded rubber-sand mixtures. *Geosynthetics International*, 1-21. Advance online publication. https://doi.org/10.1680/jgein.24.00157. For the purpose of open access, a CC BY 4.0 licence has been applied.

Nakhaei, A., Marandi, S.M., Kermani, S.S. and Bagheripour, M.H. (2012). Dynamic properties of granular soils mixed with granulated rubber. *Soil Dynamics and Earthquake Engineering*, 43, pp. 124–132. DOI: 10.1016/j.soildyn.2012.07.026.

Murillo, C., Thorel, L. and Caicedo, B. (2009). Ground vibration isolation with geofoam barriers: centrifuge modeling. *Geotextiles and Geomembranes*, 27(6), pp. 423–434. DOI: 10.1016/j.geotexmem.2009.03.006.

Nazari, N., Lindt, J.W. and Li, Y. (2014). Effect of aftershock intensity on seismic collapse fragilities. *International Journal of Reliability and Safety*, 8, p. 174. DOI: 10.1504/IJRS.2014.069526.

Otsubo, M., Towhata, I., Hayashida, T., Liu, B. and Goto, S. (2016). Shaking table tests on liquefaction mitigation of embedded lifelines by backfilling with recycled materials. *Soils and Foundations*, 56(3), pp. 365–378. DOI: 10.1016/j.sandf.2016.04.004

Pistolas, G.A., Anastasiadis, A. and Pitilakis, K. (2018). Dynamic behaviour of granular soil materials mixed with granulated rubber: effect of rubber content and granularity on the small-strain shear modulus and damping ratio. *Geotechnical and Geological Engineering*, 36(2), pp. 1267–1281. DOI: 10.1007/s10706-017-0391-9.

Pitilakis, D., Anastasiadis, A., Vratsikidis, A. (2021). Large-scale field testing of geotechnical seismic isolation of structures using gravel-rubber mixtures. *Earthquake Engng Struct Dyn*. 50, pp. 2712–2731. DOI: https://doi.org/10.1002/eqe.3468

Promputthangkoon, P. and Hyde, A.F.L. (2008). Compressibility and liquefaction potential of rubber composite soils. *International Workshop on Scrap Tire Derived Geomaterials – Opportunities and Challenges*, pp. 161–170. ISBN: 9780415460705.

Qian, J., Yao, Y., Li, J., Xiao, H. and Luo, S. (2020). Resilient properties of soil–rock mixture materials: Preliminary investigation of the effect of composition and structure. *Materials*, 13(7), pp. 1658. DOI: 10.3390/ma13071658

Rao, G.V. and Dutta, R.K. (2006). Compressibility and strength behaviour of sand-tyre chip mixtures. *Geotechnical and Geological Engineering*, 24(3), pp. 711–724. DOI: 10.1007/s10706-004-4006-x.

Rios, S., Kowalska, M. and Viana da Fonseca, A. (2021). Cyclic and dynamic behaviour of sand–rubber and clay–rubber mixtures. *Geotechnical and Geological Engineering*, 39, pp. 3449–3467. DOI: 10.1007/s10706-021-01704-3

Rouhanifar, S., Afrazi, M., Fakhimi, A., and Yazdani, M. (2020). Strength and deformation behaviour of sand-rubber mixture. *International Journal of Geotechnical Engineering, 15*, 1078-1092.

Bernal-Sanchez, J., McDougall, J., Barreto, D., Dimitriadi, V., Leak, J., & Anbazhagan, P. (2025). Influence of rubber content and particle morphology on the dynamic behaviour, liquefaction susceptibility and internal stability of shredded rubber-sand mixtures. *Geosynthetics International*, 1-21. Advance online publication. https://doi.org/10.1680/jgein.24.00157. For the purpose of open access, a CC BY 4.0 licence has been applied.

Senetakis, K., Anastasiadis, A. and Pitilakis, K. (2012). Dynamic properties of dry sand/rubber (SRm) and gravel/rubber (GRm) mixtures in a wide range of shearing strain amplitudes. *Journal of ASTM International*, 33(1), pp. 38–53. DOI: 10.1016/j.soildyn.2011.10.003.

Shariatmadari, N., Karimpour-Fard, M. and Shargh, A. (2018). Undrained monotonic and cyclic behaviour of sand-ground rubber mixtures. *Earthquake Engineering and Engineering Vibration*, 17(3), pp. 541–553. DOI: 10.1007/s11803-018-0461-x.

Sheikh, M.N., Mashiri, M.S., Vinod, J.S. and Tsang, H.H. (2012). Shear and compressibility behaviour of sand-tyre crumb mixtures. *Journal of Materials in Civil Engineering*, 25(10), pp. 1366–1374. DOI: doi.org/10.1061/(ASCE)MT.1943-5533.0000696

Signes, C.H., Garzon-Roca, J., Grima-Palop, J.M. and Insa-Franco, R. (2017). Use of rubber shreds to enhance attenuation of railway sub-ballast layers made of unbound aggregates. *Materiales de Construcción*, 67(326), pp. 1–10. DOI: 10.3989/mc.2017.00316

Spence, R.J.S., So, E. and Scawthorn, C. (2011). *Human casualties in earthquakes: progress in modelling and mitigation.*

Towhata, I. (2014). *Geotechnical Earthquake Engineering.* 1st ed., Springer Series in Geomechanics and Geoengineering, London.

Toygar, O., Ulgen, D. and Fidan, N.B. (2024). Experimental study on reutilization of waste rubber chips with sheetpiles as a coupled-wave barrier to reduce ground-borne vibrations. *Journal of Vibration Engineering & Technologies*. 12, pp. 8451–8463. DOI: 10.1007/s42417- 024-01369-1.

Tsang, H.H. (2008). Seismic isolation by rubber-soil mixtures for developing countries. *Earthquake Engineering and Structural Dynamics*, 37(2), pp. 283–303. DOI: 10.1002/eqe.756.

Tsang, H.H. (2009). Geotechnical seismic isolation. In: Miura, T. and Ikeda, Y. Earthquake Engineering: New Research. Nova Science Publishers, pp. 55–87.

Tsang, H.H., Lo, S.H., Xu, X. and Sheikh, M.N. (2012). Seismic isolation for low-to-medium rise buildings using granulated rubber-soil mixtures: numerical study. *Earthquake Engineering and Structural Dynamics*, 41(4), pp. 2009–2024. DOI: 10.1002/eqe.2171.

Tsang, H.H. and Pitilakis, K. (2019). Mechanism of geotechnical seismic isolation system: analytical modelling. *Soil Dynamics and Earthquake Engineering*, 122, pp. 171–184. DOI: 10.1016/j.soildyn.2019.03.037

Bernal-Sanchez, J., McDougall, J., Barreto, D., Dimitriadi, V., Leak, J., & Anbazhagan, P. (2025). Influence of rubber content and particle morphology on the dynamic behaviour, liquefaction susceptibility and internal stability of shredded rubber-sand mixtures. *Geosynthetics International*, 1-21. Advance online publication. https://doi.org/10.1680/jgein.24.00157. For the purpose of open access, a CC BY 4.0 licence has been applied.

Tsang, H.H., Tran, D.P., Hung, W.Y., Pitilakis, K. and Gad, E.F. (2020). Performance of geotechnical seismic isolation system using rubber-soil mixtures in centrifuge testing. *Earthquake Engineering & Structural Dynamics*, 50(5), pp. 1271–1289. DOI: 10.1002/eqe.3398.

Tsuha, C.H.C., Foray, P.Y., Jardine, R.J., Yang, Z.X., Silva, M. and Rimoy, S. (2012). Behaviour of displacement piles in sand under cyclic axial loading. *Soils and Foundations*, 52(3), pp. 393–410.

Vratsikidis, A. and Pitilakis, D. (2022). Field testing of gravel-rubber mixtures as geotechnical seismic isolation. *Bulletin of Earthquake Engineering*. DOI: 10.1007/s10518-022-01541-6. DOI: 10.1016/j.sandf.2012.05.002.

Wang, J., Wu, M., Liu, F., Bin., J., He, J. (2024). Rubber-sand infilled soilbags as seismic isolation cushions: Experimental validation. *Geotechnical Engineering, ICE*. DOI: 10.1680/jgein.23.00158.

Wu, M., Tian, W., He, J., Liu, F. and Yang, J. (2023). Seismic isolation effect of rubber-sand mixture cushion under different site classes based on a simplified analysis model. *Soil Dynamics and Earthquake Engineering*, 168. DOI: 10.1016/j.soildyn.2022.107738.

Yakovlev, I., Sztucki, M., Fleck, F., Karimi-Varzaneh, H.A., Lacayo-Pineda, J., Vatterott, C. and Giese, U. (2025). *Journal of Applied Polymer Science*, 142(4). DOI: 10.1002/app.56403

Youwai, S. and Bergado, D.T. (2003). Strength and deformation characteristics of shredded rubber tire sand mixtures. *Canadian Geotechnical Journal*, 40(2), pp. 254–264. DOI: 10.1139/t02-104.

Zornberg, J.G., Cabral, A.R. and Viratjandr, C. (2004). Behaviour of tire shred-sand mixtures. *Canadian Geotechnical Journal*, 41(2), pp. 227–241. DOI: 10.1139/t03086.

Feng, F. and Sutter, K.G. (2000). Dynamic properties of granulated rubber/sand mixtures. *Geotechnical Testing Journal*, 23(3), pp. 338–344. DO.I: 10.1520/GTJ11055J.

Bernal-Sanchez, J., McDougall, J., Barreto, D., Dimitriadi, V., Leak, J., & Anbazhagan, P. (2025). Influence of rubber content and particle morphology on the dynamic behaviour, liquefaction susceptibility and internal stability of shredded rubber-sand mixtures. *Geosynthetics International*, 1-21. Advance online publication. https://doi.org/10.1680/jgein.24.00157. For the purpose of open access, a CC BY 4.0 licence has been applied.

942

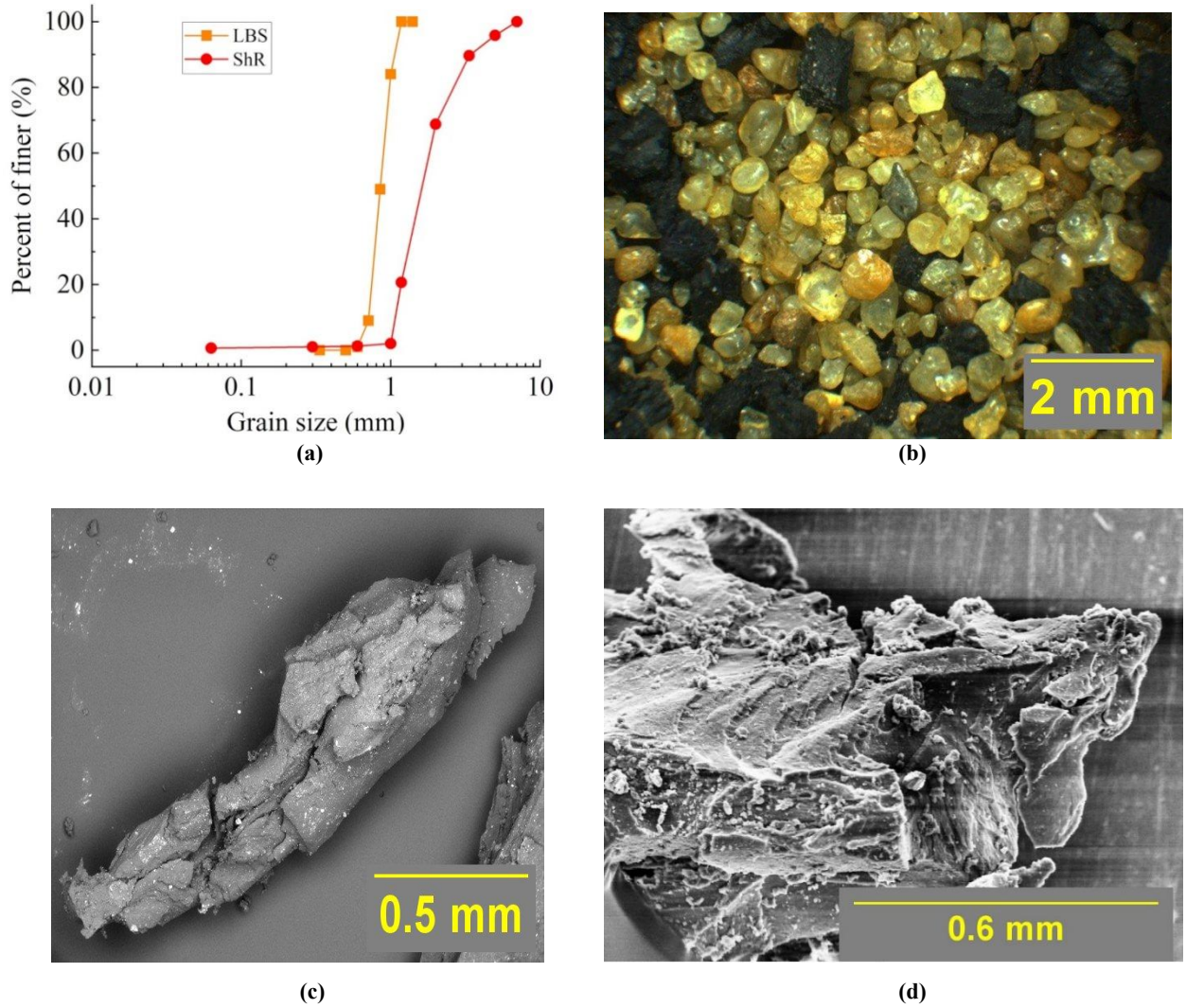

943 **(a)** **(b)**

944 **(c)** **(d)**

945 **Figure 1. a) Sieve analysis of LBS and ShR, b) microscopic image of LBS, c) microscopic image of ShR, d) fissures and**
946 **cracks on surface of ShR**

Bernal-Sanchez, J., McDougall, J., Barreto, D., Dimitriadi, V., Leak, J., & Anbazhagan, P. (2025). Influence of rubber content and particle morphology on the dynamic behaviour, liquefaction susceptibility and internal stability of shredded rubber-sand mixtures. *Geosynthetics International*, 1-21. Advance online publication. https://doi.org/10.1680/jgein.24.00157. For the purpose of open access, a CC BY 4.0 licence has been applied.

947

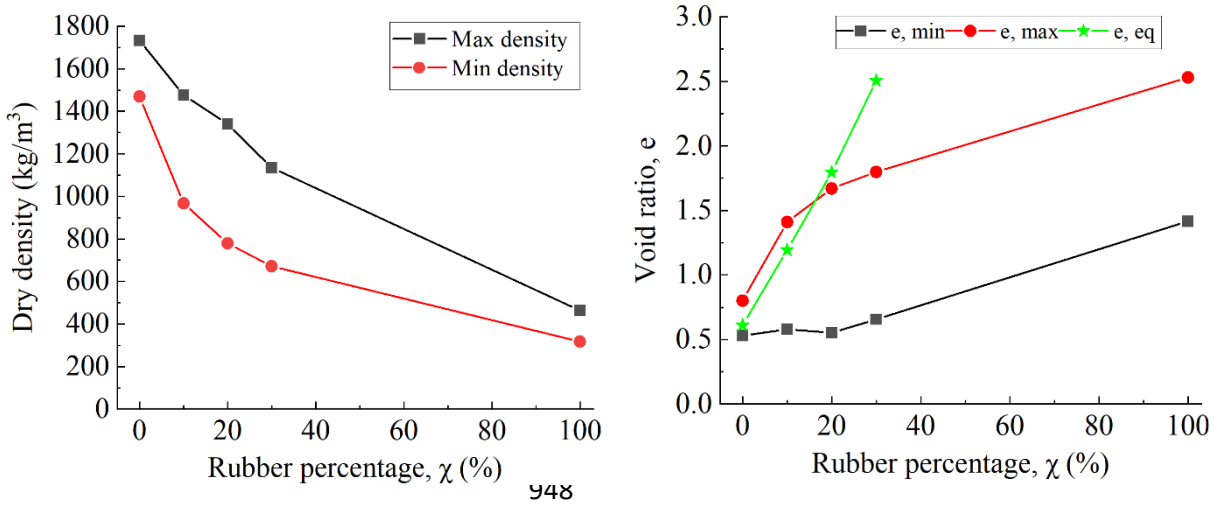

948

949 **(a)** **(b)**

950 **Figure 2. a) Min / max dry sample density, and b) Min / max void ratio per gravimetric proportion**

Bernal-Sanchez, J., McDougall, J., Barreto, D., Dimitriadi, V., Leak, J., & Anbazhagan, P. (2025). Influence of rubber content and particle morphology on the dynamic behaviour, liquefaction susceptibility and internal stability of shredded rubber-sand mixtures. *Geosynthetics International*, 1-21. Advance online publication. https://doi.org/10.1680/jgein.24.00157. For the purpose of open access, a CC BY 4.0 licence has been applied.

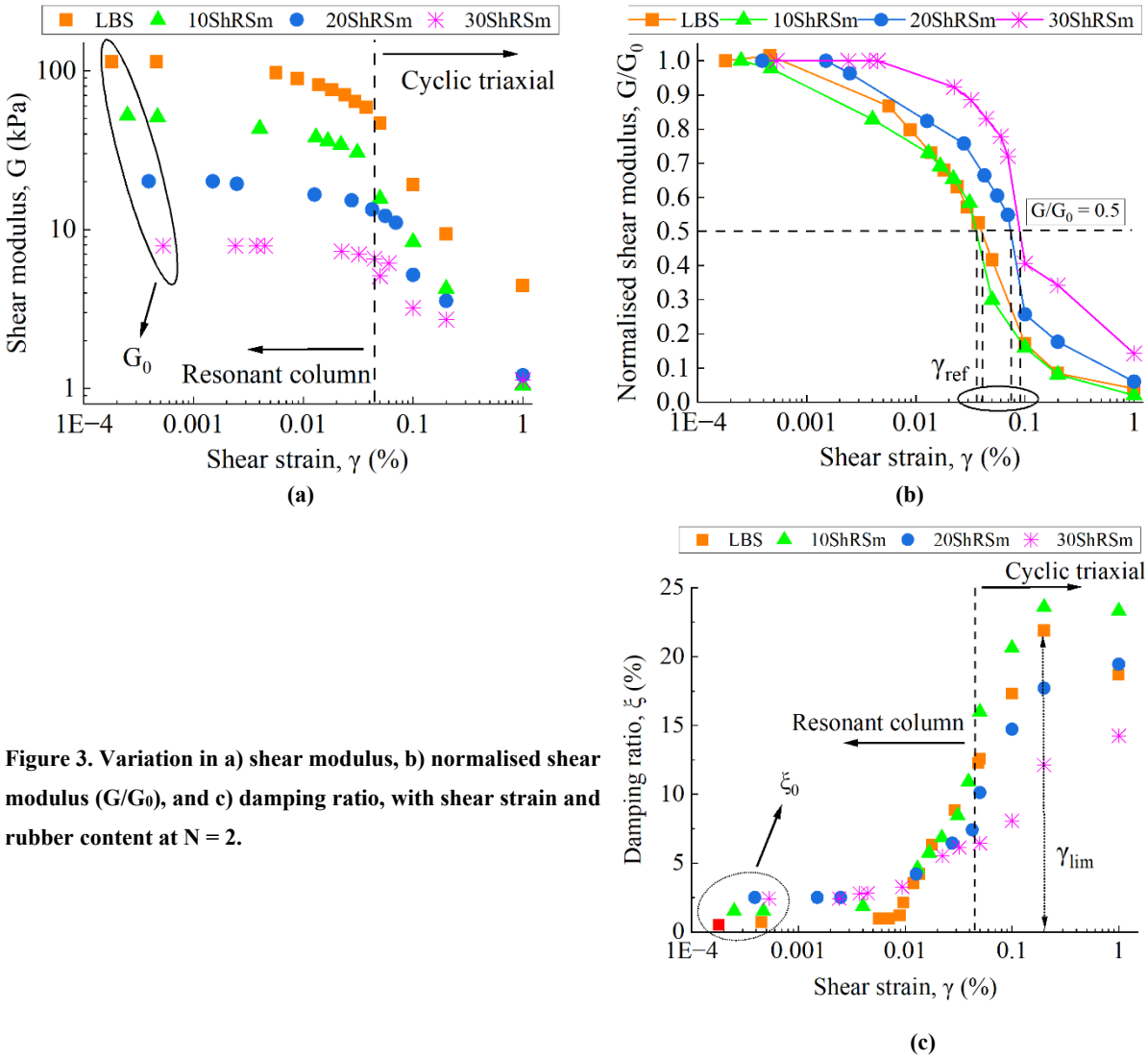

Figure 3. Variation in a) shear modulus, b) normalised shear modulus (G/G0), and c) damping ratio, with shear strain and rubber content at N = 2.

Bernal-Sanchez, J., McDougall, J., Barreto, D., Dimitriadi, V., Leak, J., & Anbazhagan, P. (2025). Influence of rubber content and particle morphology on the dynamic behaviour, liquefaction susceptibility and internal stability of shredded rubber-sand mixtures. *Geosynthetics International*, 1-21. Advance online publication. https://doi.org/10.1680/jgein.24.00157. For the purpose of open access, a CC BY 4.0 licence has been applied.

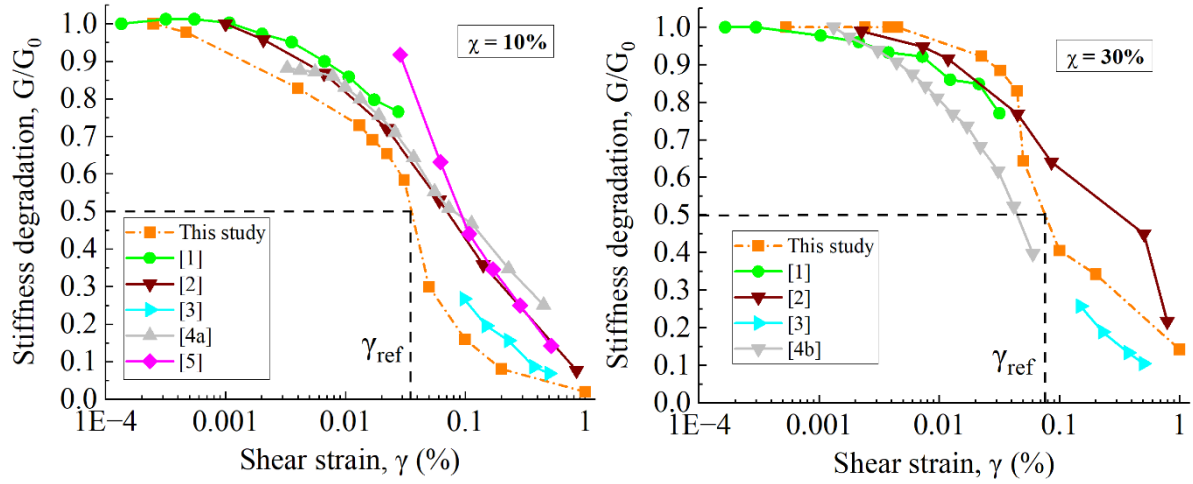

(a) (b)

Figure 4. Normalised shear modulus versus shear strain of RSm at a) χ = 10%, and b) χ = 30%. [1] = Feng & Sutter, 2000; [2] = Kaneko et al., 2013; [3] = Mashiri et al., 2016; [4a] = Pistolas et al., 2018; [4b] = Anastasiadis et al., 2012b; [5] = Nakhaei et al., 2012

Bernal-Sanchez, J., McDougall, J., Barreto, D., Dimitriadi, V., Leak, J., & Anbazhagan, P. (2025). Influence of rubber content and particle morphology on the dynamic behaviour, liquefaction susceptibility and internal stability of shredded rubber-sand mixtures. *Geosynthetics International*, 1-21. Advance online publication. https://doi.org/10.1680/jgein.24.00157. For the purpose of open access, a CC BY 4.0 licence has been applied.

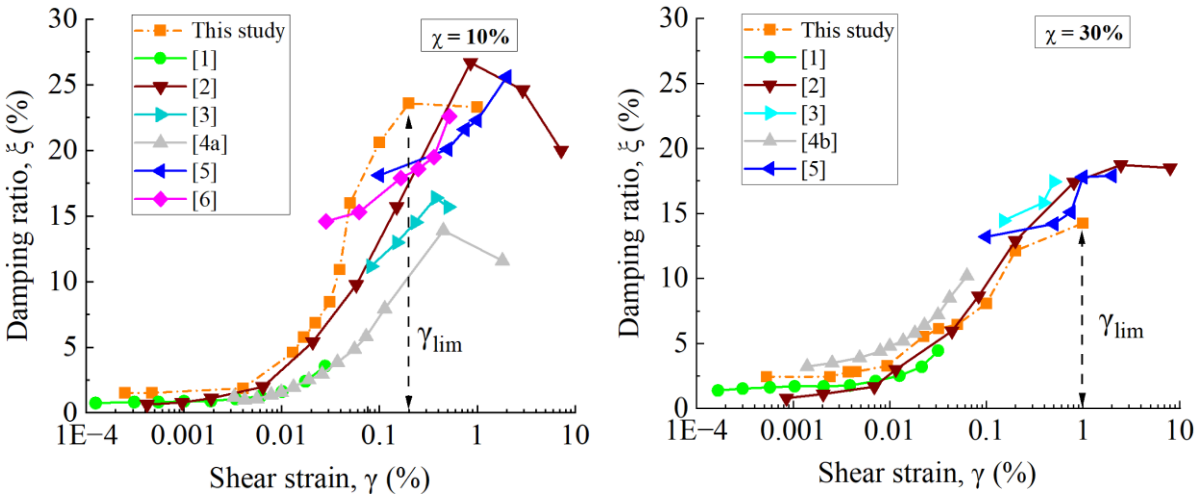

(a) (b)

Figure 5. Damping ratio versus shear strain of RSm at a) χ = 10%, and b) χ = 30%. [1] = Feng & Sutter, 2000; [2] = Kaneko et al., 2013; [3] = Mashiri et al., 2016; [4a] = Pistolas et al., 2018; [4b] = Anastasiadis et al., 2012b; [5] = Madhusudhan et al., 2019; [6] = Nakhaei et al., 2012

Bernal-Sanchez, J., McDougall, J., Barreto, D., Dimitriadi, V., Leak, J., & Anbazhagan, P. (2025). Influence of rubber content and particle morphology on the dynamic behaviour, liquefaction susceptibility and internal stability of shredded rubber-sand mixtures. *Geosynthetics International*, 1-21. Advance online publication. https://doi.org/10.1680/jgein.24.00157. For the purpose of open access, a CC BY 4.0 licence has been applied.

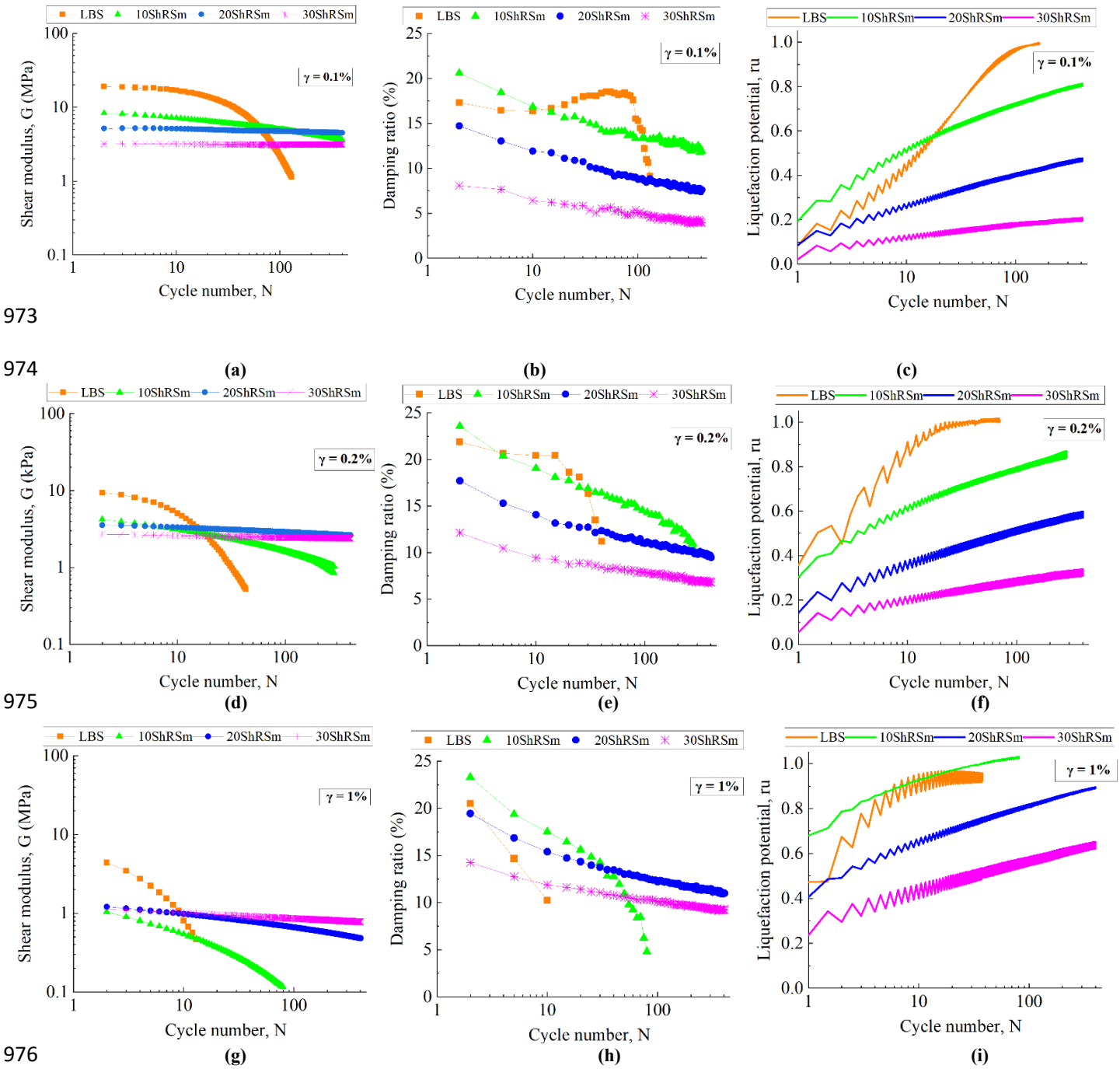

Figure 6. Evolution in shear modulus (a, d, g), damping ratio (b, e, h), and liquefaction susceptibility (c, f, i) with the cycle number at γ = 0.1, 0.2 and 1%.

Bernal-Sanchez, J., McDougall, J., Barreto, D., Dimitriadi, V., Leak, J., & Anbazhagan, P. (2025). Influence of rubber content and particle morphology on the dynamic behaviour, liquefaction susceptibility and internal stability of shredded rubber-sand mixtures. *Geosynthetics International*, 1-21. Advance online publication. https://doi.org/10.1680/jgein.24.00157. For the purpose of open access, a CC BY 4.0 licence has been applied.

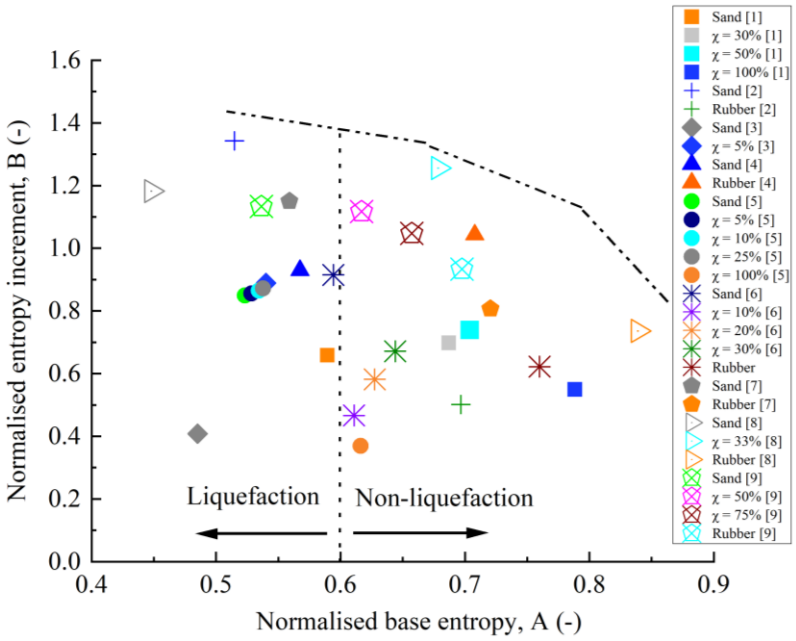

Figure 7. Internal stability of RSm adapted from Bernal-Sanchez et al. (2023): [1] = Kaneko et al., 2013; [2] = Otsubo et al., 2016; [3] = Proputthankoon and Hyde, 2008; [4] = Bahadori and Roohollah, 2018; [5] = Shariatmadari et al., 2018 [6] = Bernal-Sanchez et al., 2023, [7] = Enquan and Qiong, 2019; [8] = Rios et al., 2021; [9] = Amuthan et al., 2020

Bernal-Sanchez, J., McDougall, J., Barreto, D., Dimitriadi, V., Leak, J., & Anbazhagan, P. (2025). Influence of rubber content and particle morphology on the dynamic behaviour, liquefaction susceptibility and internal stability of shredded rubber-sand mixtures. *Geosynthetics International*, 1-21. Advance online publication. https://doi.org/10.1680/jgein.24.00157. For the purpose of open access, a CC BY 4.0 licence has been applied.

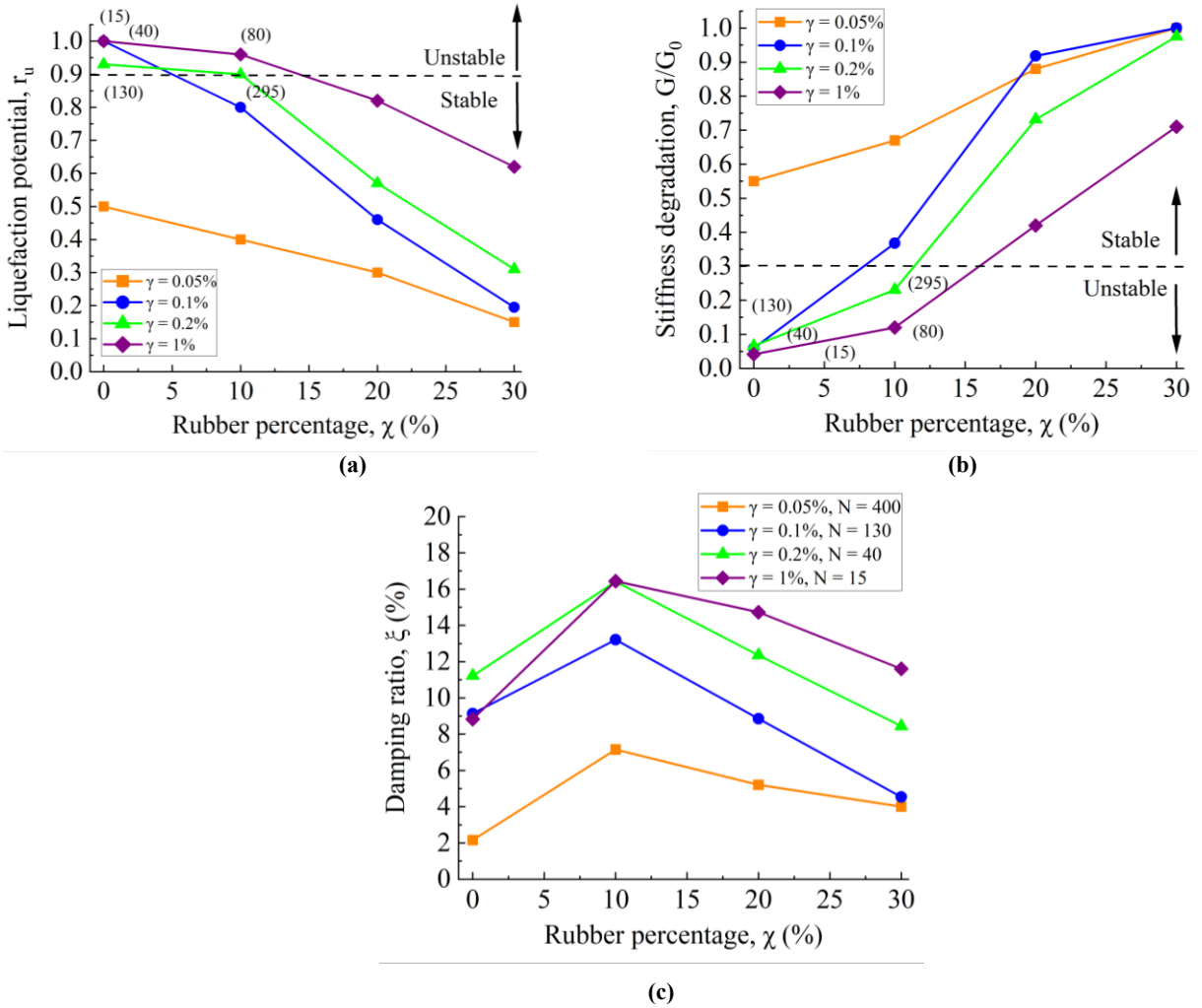

Figure 8. a) Pore pressure ratio, b) stiffness degradation and c) damping ratio with strain amplitude and number of cycles to liquefaction (in parenthesis when less than N = 400)

Bernal-Sanchez, J., McDougall, J., Barreto, D., Dimitriadi, V., Leak, J., & Anbazhagan, P. (2025). Influence of rubber content and particle morphology on the dynamic behaviour, liquefaction susceptibility and internal stability of shredded rubber-sand mixtures. *Geosynthetics International*, 1-21. Advance online publication. https://doi.org/10.1680/jgein.24.00157. For the purpose of open access, a CC BY 4.0 licence has been applied.

1013 **Table 1. Material properties of LBS and shredded rubber particles**

Material properties	LBS	ShR
Effective size, D_{10} (mm)	0.71	1.05
D_{30} (mm)	0.8	1.31
Mean size, D_{50} (mm)	0.86	1.62
D_{60} (mm)	0.89	1.78
Size ratio, SR	-	1.88
Aspect ratio, A_r	1	2-6
Sphericity	0.65	0.18
Roundness	0.78	0.82
Coefficient of uniformity, C_u	1.25	1.44
Coefficient of curvature, C_c	1.01	1.78
Specific gravity	2.68	1.12
Coefficient of friction, μ	0.24	1

1014

Bernal-Sanchez, J., McDougall, J., Barreto, D., Dimitriadi, V., Leak, J., & Anbazhagan, P. (2025). Influence of rubber content and particle morphology on the dynamic behaviour, liquefaction susceptibility and internal stability of shredded rubber-sand mixtures. *Geosynthetics International*, 1-21. Advance online publication. https://doi.org/10.1680/jgein.24.00157. For the purpose of open access, a CC BY 4.0 licence has been applied.

1015 **Table 2. Classification of experimental programme using both resonant column and cyclic triaxial equipment**

Test ID	χ (%)	Strain amplitude, γ (%)	Sample void ratio, e_{sample}	Relative density, D_r (%)	Number of cycles, N
LBS-RC	0	$1.8 \times 10^{-4} – 5.3 \times 10^{-2}$	0.61	70.3	-
LBS-0.05	0	0.05	0.60	74.0	400
LBS-0.1	0	0.1	0.59	77.7	100 (Liquified)
LBS-0.2	0	0.2	0.60	74.0	41 (LQ)
LBS-1	0	1	0.59	77.7	14 (LQ)
10ShRSm-RC	10	$2.5 \times 10^{-4} – 4.7 \times 10^{-2}$	0.79	74.6	-
10ShRSm-0.05	10	0.05	0.73	81.7	400
10ShRSm-0.1	10	0.1	0.75	79.4	240 (LQ)
10ShRSm-0.2	10	0.2	0.76	78.2	50 (LQ)
10ShRSm-1	10	1	0.77	77.0	400
20ShRSm-RC	20	$3.9 \times 10^{-4} – 5.6 \times 10^{-2}$	0.81	76.9	-
20ShRSm-0.05	20	0.05	0.74	83.2	400
20ShRSm-0.1	20	0.1	0.78	79.6	400
20ShRSm-0.2	20	0.2	0.76	81.4	400
20ShRSm-1	20	1	0.80	77.8	400
30ShRSm-RC	30	$5.3 \times 10^{-4} – 6 \times 10^{-2}$	0.82	85.0	-
30ShRSm-0.05	30	0.05	0.83	84.8	400
30ShRSm-0.1	30	0.1	0.85	83.0	400
30ShRSm-0.2	30	0.2	0.84	83.9	400
30ShRSm-1	30	1	0.86	82.1	400

1016

Bernal-Sanchez, J., McDougall, J., Barreto, D., Dimitriadi, V., Leak, J., & Anbazhagan, P. (2025). Influence of rubber content and particle morphology on the dynamic behaviour, liquefaction susceptibility and internal stability of shredded rubber-sand mixtures. *Geosynthetics International*, 1-21. Advance online publication. https://doi.org/10.1680/jgein.24.00157. For the purpose of open access, a CC BY 4.0 licence has been applied.

1017

1018 **Table 3:** Studies on response of RSm under dynamic loading

Reference	Apparatus	RC (%)	Sample state	γ_a (%)	$D_{R50sand}$ (mm)	$D_{50rubber}$ (mm)	SR	D_r (%)	N	σ_m (kPa)
Feng and Sutter (2000)	RC	V = 29 - 100	D	0.0001 - 0.05	0.6 - 0.8	RF; 2 - 4.76	4 - 6	NS	NT	69 - 483
Nakhaei et al. (2012)	CT	χ = 0 - 14	D	0.0001	0.6 - 0.85	GR; 0.6 - 0.92	1	NS	NT	34 - 207
Anastasiadis et al. (2012b)	RC	χ = 0 - 35	D	0.0001-0.02	0.27 - 7.8	GR; 0.34 - 2.8	0.3 - 1	NT	< 10	50 - 400
Kaneko et al. (2013)	OT	V = 0, 30, 50	S	EMs	0.4	TCh; 0.7	2	50	Vr.	NS
Mashiri et al. (2016)	CT	χ = 0 - 40	SUC	0.15 - 0.5	0.35	TCh; 5	15	50	100	23 - 138
Li et al. (2016)	RC, CT	V = 0 - 20	SDC	CSR = 0.2	0.8	GR; 0.12	1 - 4	NS	50	50 - 200
Pistolas et al. (2018)	CT, RC	χ = 0 - 60	S	0.01 - 2	0.41	GR; 1.55 - 3.38	4 - 8	e = 0.7	2	25 - 200
Madhusudhan et al. (2019)	CT	χ = 0 - 100	D	0.1 - 2	2	TSh; 2	1	65 - 80	100	100
This study	RC, CT	χ = 0 - 30	S	0.0001 – 1	0.86	ShR; 1.62	1.88	65-80	400	100

1019 Note: CT = Cyclic Triaxial, RC = Resonant Column; OT = Online test; χ = Gravimetric proportion; V = volumetric proportion; SUC = Saturated undrained consolidated;
1020 SDC = Saturated drained consolidated; D = Dry; S = Saturated; γ_a = Shear strain amplitude; EMs = earthquake motions; GR = granulated rubber; RF = Rubber fibres; ShR =
1021 Shredded Rubber; TSh; Tyre shreds; TCh = Tyre chips; SR = dR50/dS50; e = void ratio; σ_m = Cell pressure; D_r = Relative density; NS = Not specified; NT = Not tested; Vr =
1022 Variable

1023

Bernal-Sanchez, J., McDougall, J., Barreto, D., Dimitriadi, V., Leak, J., & Anbazhagan, P. (2025). Influence of rubber content and particle morphology on the dynamic behaviour, liquefaction susceptibility and internal stability of shredded rubber-sand mixtures. *Geosynthetics International*, 1-21. Advance online publication. https://doi.org/10.1680/jgein.24.00157. For the purpose of open access, a CC BY 4.0 licence has been applied.

1024 **Table 4. Stiffness and damping degradation with respect to cycle number, rubber content and strain amplitude**

Strain amplitude, γ (%)	χ (%)	Number of cycles, N	Stiffness degradation (%)	Damping degradation (%)
0.1	0	20	-27.6	-1.3
		40	-52.3	4.4
		130	-94.1	-47.2
		400	Liquified (LQ)	LQ
0.1	10	20	-22.0	-24.0
		40	-29.7	-28.2
		130	-43.3	-35.9
		400	-56.6	-41.7
0.1	20	20	-3.3	-24.5
		40	-6.5	-32.0
		130	-8.8	-39.9
		400	-12.6	-48.5
0.1	30	20	-0.9	-25.2
		40	-2.7	-37.3
		130	-2.0	-43.8
		400	-2.3	-51.4
0.2	0	20	-75.4	-14.9
		40	-93.4	-48.7
		130	LQ	LQ
		400	LQ	LQ
0.2	10	20	-37.1	-24.8
		40	-48.0	-30.4
		130	-64.9	-40.6
		400	LQ	LQ
0.2	20	20	-10.2	-26.7

Bernal-Sanchez, J., McDougall, J., Barreto, D., Dimitriadi, V., Leak, J., & Anbazhagan, P. (2025). Influence of rubber content and particle morphology on the dynamic behaviour, liquefaction susceptibility and internal stability of shredded rubber-sand mixtures. *Geosynthetics International*, 1-21. Advance online publication. https://doi.org/10.1680/jgein.24.00157. For the purpose of open access, a CC BY 4.0 licence has been applied.

		40	-13.7	-30.2
		130	-19.8	-39.1
		400	-26.0	-45.6
0.2	30	20	-5.3	-27.7
		40	-7.5	-30.4
		130	-9.7	-36.4
		400	-10.9	-43.8
1	0	20	LQ	LQ
		40	LQ	LQ
		130	LQ	LQ
		400	LQ	LQ
1	10	20	-64.4	-33.0
		40	-78.4	-45.2
		130	LQ	LQ
		400	LQ	LQ
1	20	20	-26.6	-26.2
		40	-34.7	-30.8
		130	-48.0	-38.0
		400	-60.0	-43.6
1	30	20	-14.4	-19.8
		40	-18.7	-24.3
		130	-25.0	-29.7
		400	-30.8	-34.8

1025